

GSFIXER: IMPROVING 3D GAUSSIAN SPLATTING WITH REFERENCE-GUIDED VIDEO DIFFUSION PRIORS

Xingyilang Yin^{1,2†*} Qi Zhang^{2†} Jiahao Chang³ Ying Feng²
 Qingnan Fan² Xi Yang⁴ Chi-Man Pun^{1‡} Huaqi Zhang² Xiaodong Cun^{5‡}
¹University of Macau ²VIVO ³CUHKSZ ⁴Xidian University ⁵GVC Lab, Great Bay University

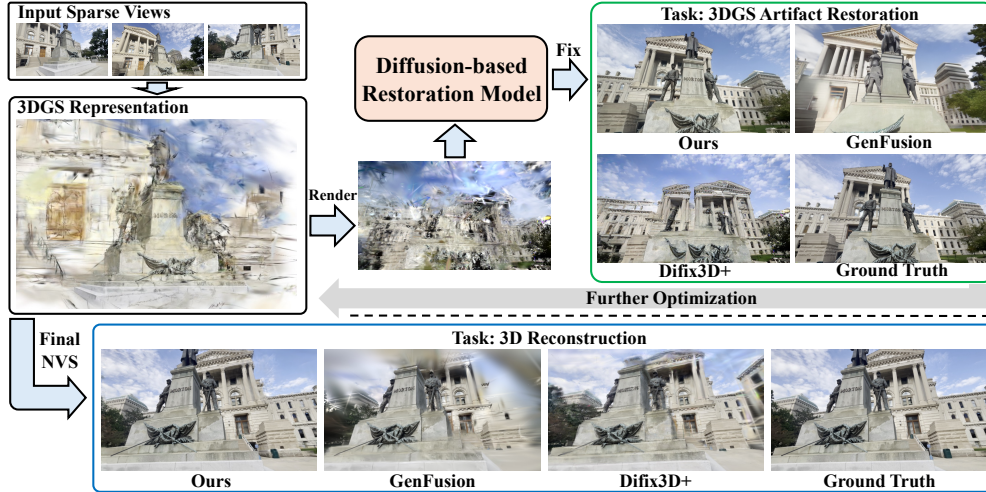


Figure 1: We introduce GSFixer, a framework capable of improving 3DGS in both artifact restoration (top) and 3D reconstruction (bottom) under sparse-view settings. Recent generative methods struggle with maintaining consistency between generated and input views. GSFixer guides the video diffusion model conditioned on both 3D and 2D signals to enhance consistency in novel view restoration, thereby improving 3D reconstruction quality.

ABSTRACT

Reconstructing 3D scenes using 3D Gaussian Splatting (3DGS) from sparse views is an ill-posed problem due to insufficient information, often resulting in noticeable artifacts. While recent approaches have sought to leverage generative priors to complete information for under-constrained regions, they struggle to generate content that remains consistent with input observations. To address this challenge, we propose **GSFixer**, a novel framework designed to improve the quality of 3DGS representations reconstructed from sparse inputs. The core of our approach is the reference-guided video restoration model, built upon a DiT-based video diffusion model trained on paired artifact 3DGS renders and clean frames with additional reference-based conditions. Considering the input sparse views as references, our model integrates both 2D semantic features and 3D geometric features of reference views extracted from the visual geometry foundation model, enhancing the semantic coherence and 3D consistency when fixing artifact novel views. Furthermore, considering the lack of suitable benchmarks for 3DGS artifact restoration evaluation, we present DL3DV-Res which contains artifact frames rendered using low-quality 3DGS. Extensive experiments demonstrate our GSFixer outperforms current state-of-the-art methods in 3DGS artifact restoration and sparse-view 3D reconstruction. Project page: <https://github.com/GVCLab/GSFixer>.

*Work done during an internship at VIVO. † Equal contribution. ‡ Corresponding authors.

1 INTRODUCTION

3D reconstruction and novel view synthesis (NVS) are fundamental tasks in computer vision and graphics, with wide-ranging real-world applications in virtual reality, autonomous driving, and robotics. Recently, 3D Gaussian Splatting (3DGS) (Kerbl et al., 2023) has achieved impressive results in both reconstruction quality and rendering efficiency when dense input views are available. However, its performance degrades significantly in sparse-view settings, where limited viewpoint information leads to under-constrained 3D representations. In such cases, 3DGS often suffers from severe artifacts, including distorted geometric structures and incomplete reconstructions, particularly in less-observed regions or extreme novel viewpoints. These limitations hinder its applicability in real-world scenarios where acquiring dense multi-view data is challenging.

To alleviate the limitations, some previous regularization methods have been proposed to introduce additional constraints into the 3DGS optimization process, such as monocular depth (Li et al., 2024; Zhu et al., 2024), frequency smoothness (Zhang et al., 2024), and random dropout (Xu et al., 2025). While these approaches can help prevent 3DGS representations from overfitting to sparse input views, they often remain sensitive to noise and yield only marginal improvements in NVS rendering quality. Inspired by the success of ReconFusion (Wu et al., 2024), which introduces diffusion model into NeRF (Mildenhall et al., 2020) optimization, more recent studies (Liu et al., 2024b;a; Wu et al., 2025a;b) explore incorporating 3DGS optimization with powerful generative priors from diffusion models, which are trained on internet-scale data. These strong priors enable the correction of spurious geometry or the inpainting of plausible content in novel views. However, a key challenge still remains: maintaining visual and 3D consistency between the generated and original input images, especially when the novel views are far from the observed inputs.

Meanwhile, recent advances in controllable video generation have demonstrated the effectiveness of incorporating various conditional signals (Niu et al., 2024; Hu, 2024; He et al., 2025; Cui et al., 2025; YU et al., 2025) to guide video diffusion models in generating high-quality and coherent content. This progress motivates us to investigate appropriate control conditions to guide the video diffusion model in restoring artifact-ridden novel views, aiming for enhanced visual quality and 3D consistency. Given that the input to the sparse-view reconstruction task consists of only a few images—treated as ground-truth views—it is natural to align the restored novel views with these inputs. Thus, we exploit the information from reference views within the input set to condition the video diffusion model. Since artifacts manifest in 2D image space, their correction should rely on 2D visual priors to ensure semantic consistency with the reference views. At the same time, these artifacts originate from inaccurate 3DGS representations in 3D space, suggesting that effective restoration should also consider 3D structure. Therefore, an effective controllable video diffusion model for this task needs to integrate both 2D and 3D priors from reference views.

Inspired by the above motivation, we propose **GSFixer**, a novel generative reconstruction framework built upon a DiT-based video diffusion model (Yang et al., 2024), trained on paired artifact 3DGS renders and clean frames, conditioned on additional reference-based conditions. Our key insight is to leverage information of reference views to guide the video diffusion model to restore artifact-prone novel views in a geometrically consistent and visually faithful manner. This enables high-quality novel view restoration and 3D reconstruction, as shown in Figure 1. Specifically, we extract tokens via visual encoders (*e.g.*, DINOv2 (Oquab et al., 2024)) as 2D semantic signal to ensure semantic consistency between the fixed novel views and the input observations. To further enforce multi-view consistency, we incorporate features from feed-forward 3D reconstruction networks (*e.g.*, VGGT (Wang et al., 2025)) as 3D geometric condition. Moreover, we introduce a reference trajectory sampling strategy into the iterative generative optimization process to fix artifacts in novel views, effectively balancing angular coverage and restoration quality. In addition, to facilitate the evaluation of artifact removal capabilities of generative methods, we present DL3DV-Res, a benchmark comprising artifact-ridden frames rendered from low-quality 3DGS representations. Empirical results demonstrate that our GSFixer achieves superior sparse-view restoration and reconstruction performance on various challenging scenes.

Our main contributions are summarized as follows:

- We introduce GSFixer, a novel generative reconstruction framework tailored for improving the quality of 3DGS representations. It integrates a reference-guided video restoration model along with a reference-guided trajectory sampling strategy.

- We propose to incorporate video diffusion model conditioned on both 2D semantic and 3D geometric features extracted from the reference views. This effectively guides the restoration of artifact novel views, achieving both semantically coherent and 3D consistent results.
- We present DL3DV-Res benchmark for evaluating the performance of existing generative models in 3DGS artifact restoration. Extensive experiments demonstrate that our GSFixer outperforms existing baselines in video-based 3D artifact restoration and sparse-view 3D reconstruction.

2 RELATED WORKS

Regularization Sparse-view Novel View Synthesis. Neural Radiance Fields (NeRF) and 3DGS have revolutionized the field of NVS by leveraging advances in neural rendering. While NeRF and 3DGS achieve remarkable photorealistic novel-view synthesis results given dense input views, they often suffer from severe overfitting issues and significant artifacts when training with sparse views. Previous works have attempted to address this limitation by introducing additional constraints and regularization into the per-scene 3D optimize process, such as depth supervision (Deng et al., 2022; Roessle et al., 2022; Wang et al., 2023; Li et al., 2024; Zhu et al., 2024), normal consistency (Yu et al., 2022; Seo et al., 2023), smoothness priors (Niemeyer et al., 2022; Yang et al., 2023; Zhang et al., 2024), semantic coherence (Jain et al., 2021; Truong et al., 2023), and random dropout strategy (Xu et al., 2025). However, these approaches often yield marginal improvements and remain sensitive to some specific scene data.

Conditional Video Diffusion Models. Recently, generative models (Rombach et al., 2022; Liu et al., 2023; Blattmann et al., 2023; Chen et al., 2023; 2024; Xing et al., 2024; Yang et al., 2024) have advanced rapidly and demonstrate impressive capabilities in high-quality visual content generation. Building on this progress, recent efforts have extended video diffusion models with various control signals, such as depth (Hu et al., 2025; Zhao et al., 2024), trajectory (Niu et al., 2024; YU et al., 2025), audio (Cui et al., 2025; Kong et al., 2025), camera parameters (Wang et al., 2024; Zhang et al., 2025), and point cloud renderings (Yu et al., 2024; Gu et al., 2025). The additional control signals enable the diffusion models to generate coherent content with the user’s inputs. Our work builds upon a video diffusion framework that leverages 3DGS renderings and features from clean reference frames as condition signals to guide the restoration of artifacts in novel views.

Generative Sparse-view Novel View Synthesis. Generative models have demonstrated strong ability to inpaint plausible content in unobserved regions and restore degraded areas with high visual fidelity. Recent approaches (Wu et al., 2024; Liu et al., 2024b;a; Wu et al., 2025a; Bao et al., 2025; Wu et al., 2025b) have made notable progress in the sparse-view NVS task by leveraging priors from generative models. For instance, ReconFusion (Wu et al., 2024) combines image diffusion with PixelNeRF (Yu et al., 2021) as condition to optimize NeRF representations. Similarly, more recent works (Liu et al., 2024b; Wu et al., 2025a; Bao et al., 2025; Wu et al., 2025b) utilize diffusion priors to enhance low-quality 3DGS representations. Our work is closely related to 3DGS-Enhancer (Liu et al., 2024b), GenFusion (Wu et al., 2025b) and DIFIX3D+ (Wu et al., 2025a), all of which finetune diffusion models to correct artifacts in novel views. While following a similar direction, our method differs in two key aspects: (i) we finetune a DiT-based video diffusion model controlled with additional reference view conditions, and (ii) we incorporate both 2D semantic features and 3D geometric features extracted from visual geometry foundation models to guide the video restoration process, effectively fixing the artifacts in novel views.

3 METHODS

3.1 PRELIMINARY

3D Gaussian Splatting and Novel View Synthesis. 3DGS (Kerbl et al., 2023) explicitly represents a 3D scene as a collection of 3D Gaussian spheres, enabling high-quality 3d reconstructions and efficient novel view synthesis. Each 3D Gaussian sphere is defined by its center location μ , scaling vector s , rotation quaternion q , opacity σ , and spherical harmonic (SH) coefficients sh . Thus, the Gaussian distribution is formulated as:

$$G(x) = e^{-\frac{1}{2}(x-\mu)^T \Sigma^{-1}(x-\mu)}, \quad (1)$$

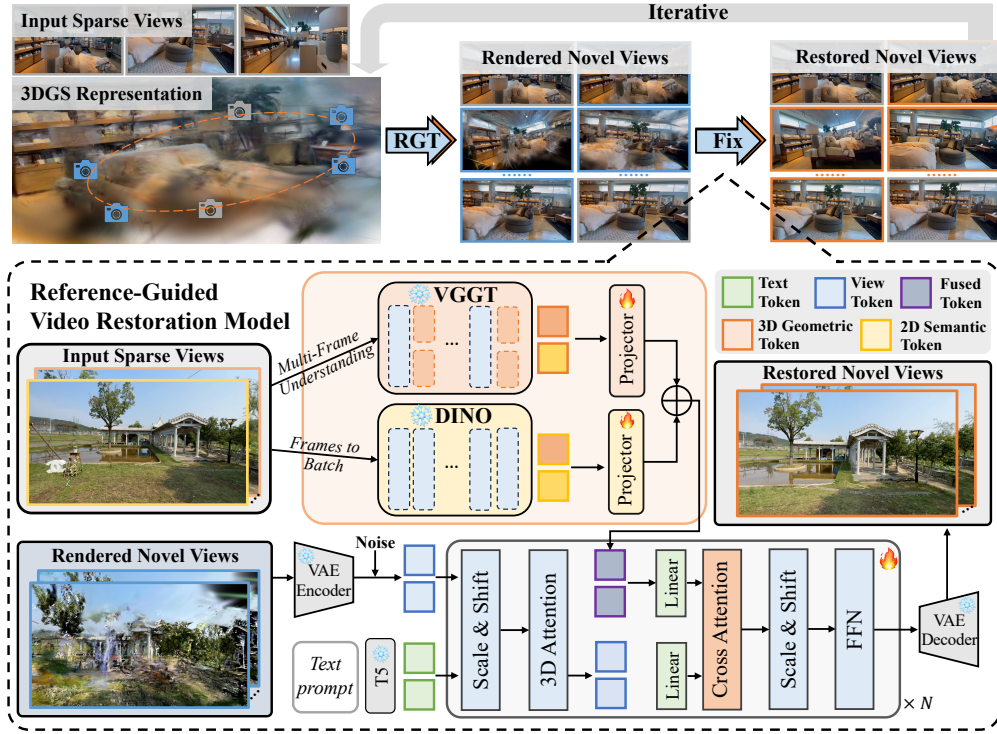


Figure 2: **Pipeline of GSFixer.** Given sparse-view images and their corresponding low-quality 3DGS representation, we render artifact-prone novel views between two reference views along a reference-guided trajectory. These novel views are fed into reference-guided video restoration model to correct artifacts, and the fixed novel views are then distilled back into the 3DGS representation to improve its quality. The restoration network is finetuned from CogVideoX and trained on paired artifact-ridden 3DGS renders and ground truth frames. It is additionally conditioned on 3D geometric tokens and 2D semantic tokens extracted from the reference views using pretrained VGGT and DINOv2 encoder, respectively.

where $\Sigma = RSS^T R^T$, S denotes the scaling matrix corresponding to s and R is the rotation matrix determined by q . For rendering novel views, volume rendering integrates these elements using:

$$C = \sum_{i \in M} c_i \alpha_i \prod_{j=1}^{i-1} (1 - \alpha_j), \quad (2)$$

where C represents the final pixel color, which is computed via alpha blending of the view-dependent colors c_i of the M contributing Gaussians, weighted by their opacities α_i .

Video Diffusion Model. Video diffusion models (Blattmann et al., 2023; Chen et al., 2023; 2024; Xing et al., 2024) typically consist of two key stages: a forward diffusion process, which progressively inject noise ϵ into clean video data $\mathbf{x}_0 \in \mathbb{R}^{n \times 3 \times h \times w}$, yielding noisy samples $\mathbf{x}_t = \alpha_t \mathbf{x}_0 + \sigma_t \epsilon$ at each time step t ; and a reverse denoising process p_θ , where a noise predictor ϵ_θ learns to recover the original data by removing the noise. This predictor was traditionally implemented using a U-Net architecture and is trained to minimize the following denoising objective:

$$\min_{\theta} \mathbb{E}_{t \sim \mathcal{U}(0,1), \epsilon \sim \mathcal{N}(\mathbf{0}, \mathbf{I})} [\|\epsilon_\theta(\mathbf{x}_t, t) - \epsilon\|_2^2]. \quad (3)$$

Following Sora (Brooks et al., 2024), recent approaches (Yang et al., 2024; Wan et al., 2025) adopt the Diffusion Transformer (DiT) (Peebles & Xie, 2023) architecture for the noise predictor. During training, a pretrained 3D VAE encoder \mathcal{E} compresses videos into latent space $\mathbf{z} = \mathcal{E}(\mathbf{x})$. These latent tokens \mathbf{z} are then patchified, concatenated with text tokens, and fed into the DiT. At inference time, the model progressively denoises the latent tokens into clean tokens, which are subsequently decoded by the 3D VAE decoder \mathcal{D} to generate the final video $\hat{\mathbf{x}} = \mathcal{D}(\mathbf{z})$.

3.2 OVERVIEW OF GSFIXER

The illustration of our GSFixer framework is depicted in Figure 2. Given K sparse-view RGB images $\{I_i\}_{i=1,\dots,K}$, camera poses $\{P_i\}_{i=1,\dots,K}$, and corresponding trained 3DGS representation of the scene, our goal is to fix the artifacts present in novel views rendered by the low-quality 3DGS representation. We fix the artifact of novel views using our reference-guided video restoration model and distill the fixed images back into the 3DGS representation to improve its quality. In our reference-guided video restoration model, we employ a visual encoder E_v and a spatial encoder E_s to respectively extract 2D semantic tokens T_{2D} and 3D geometry tokens T_{3D} from the reference views $\{I_r^{ref}\}_{r=1,\dots,K}$ (Sec. 3.3). These tokens are subsequently projected, fused and injected into a video diffusion process to guide the restoration of artifact-ridden novel views, preserving both semantic fidelity and 3D consistency with the input views (Sec. 3.3). Moreover, we introduce a reference-guided trajectory sampling strategy within the iterative generative optimization to further enhance the quality. (Sec. 3.4).

3.3 REFERENCE-GUIDED VIDEO RESTORATION MODEL

Motivation. Recent works (Liu et al., 2024b; Wu et al., 2025b) have introduced video diffusion priors to restore artifact-prone novel views into clean frames. However, the generated frames often lack visual and 3D consistency with the input sparse views, leading to suboptimal 3D reconstruction performance. To address this, considering the artifacts finally lie in the 2D image space and are caused by suboptimal 3DGS representations in 3D space, we propose injecting both 2D semantic and 3D geometric control signals of reference views to guide the video diffusion process, enabling semantic and 3D consistency in restoring the artifact novel views.

As illustrated in Figure 2, our reference-guided video restoration model is built upon DiT-based video diffusion model CogVideoX (Yang et al., 2024), an image-to-video diffusion model capable of animating an input image to generate a video. We utilize its 3D Variational Autoencoder (VAE) for video compression and decompression. Additionally, we use BLIP (Li et al., 2022) and T5 (Raffel et al., 2020) encoder to caption video and extract the text tokens t_i^{1D} .

In our video-to-video restoration task, which aims to restore artifact frames into clean ones, we replace the original image condition with the 3DGS renders $\{I_n^{nov}\}_{n=1,\dots,N}$ between two reference views $\{I_i, I_j\}$. Both the artifact frames and reference views are encoded using the 3D VAE encoder \mathcal{E} , concatenated with per-frame initial noise, and projected into view tokens t^{view} . These view tokens are then combined with text tokens t^{text} and fed into the DiT blocks for denoising.

Reference-based Conditions. Given a set of sparse input images, we select two images $\{I_i, I_j\}$ as reference views, a set of novel views $\{I_n^{nov}\}_{n=1,\dots,N}$ along arbitrary trajectories between them, we aim to learn a conditional $\mathbf{x} \sim p(\mathbf{x}^{I^{nov}}, \{I_i, I_j\})$ to guide the video diffusion model. To incorporate 2D semantic guidance into the video diffusion process, we employ a pretrained DINOv2 (Oquab et al., 2024) model as a 2D visual tokenizer. For each reference view I_i , DINOv2 encoder \mathcal{E}_{2D} divides it into L patches and extracts robust 2D visual features as a sequence of tokens:

$$t_i^{2D} = \mathcal{E}_{2D}(I_i), t_i^{2D} \in \mathbb{R}^{L \times C}, \quad (4)$$

where t_i^{2D} denotes the resulting 2D semantic tokens, with L and C representing the number of tokens and the feature dimension, respectively.

To further control our video diffusion with 3D geometric priors, we adopt the pretrained Visual Geometry Grounded Transformer (VGGT) (Wang et al., 2025) as 3D geometric tokenizer. VGGT employs a 3D geometric encoder \mathcal{E}_{3D} , which composes several frame-wise and global self-attention layers, to encode multi-view reference views $\{I_i, I_j\}$:

$$t_i^{3D}, t_j^{3D} = \mathcal{E}_{3D}(I_i, I_j), t_i^{3D} \in \mathbb{R}^{L \times C}, t_j^{3D} \in \mathbb{R}^{L \times C}, \quad (5)$$

where t_i^{3D}, t_j^{3D} represents the extracted 3D geometric tokens, with L and C representing the number of tokens and the feature dimension, respectively. VGGT leverages these tokens to produce all key 3D attributes of a scene, including camera parameters, depth maps, point maps, and 3D point tracks through various prediction heads. Consequently, the 3D geometric tokens include rich and robust 3D geometric priors of the scene.

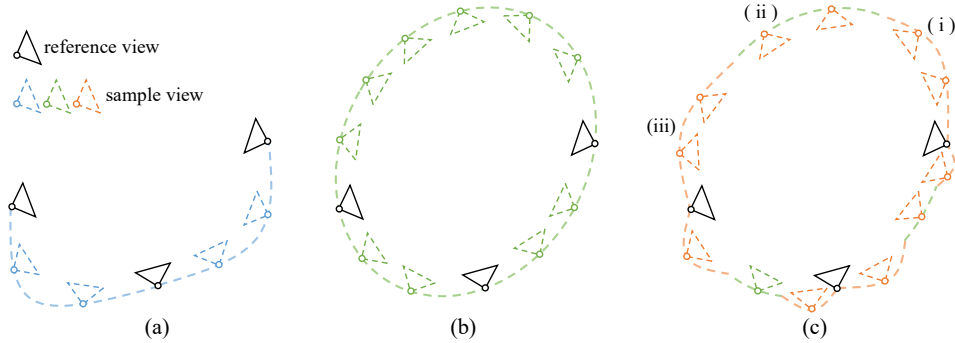


Figure 3: **Illustration of different trajectories.** (a) Interpolation trajectory: blue curve. (b) Ellipse trajectory: green curve. (c) Reference-guided trajectory: orange and green curve.

Reference-guided Generation. As previously mentioned, the fixed frames may still lack visual and 3D consistency with the reference images. To address this, we fuse 3D geometric tokens and 2D semantic tokens of reference views to fusion tokens as additional condition:

$$t_i^{fusion} = Projector_{3D}(t_i^{3D}) + Projector_{2D}(t_i^{2D}), \quad (6)$$

where $Projector_{3D}$ and $Projector_{2D}$ are implemented using linear and normalization layers.

To inject the reference fusion tokens to control the video diffusion process, we augment each DiT block by adding cross-attention layer after the 3D attention layer. In this cross-attention mechanism, the view tokens serve as queries, while the fusion tokens act as keys and values:

$$t^{view} = CrossAttention(t^{view}, t^{fusion}). \quad (7)$$

This allows the rich 2D and 3D information from the reference fusion tokens to be effectively injected into the view tokens, enabling direct alignment with the reference views and enhancing both semantic and geometric consistency when restoring artifact-prone novel views to clean ones.

3.4 REFERENCE-GUIDED GENERATIVE RECONSTRUCTION

Given rendered artifact-prone novel views and reference views, our trained reference-guided restoration diffusion model can produce consistent, artifact-free frames aligned with the input sparse views. Leveraging this capability, we supervise 3DGS optimization using both the input sparse views and the fixed novel views in an iterative training manner Haque et al. (2023); Wu et al. (2025b;a). Specifically, we begin by constructing an initial low-quality 3DGS representation from the sparse views. We then render novel views along new camera trajectories and feed these artifact-prone frames into our reference-guided video restoration model to obtain artifact-free outputs, as illustrated in Figure 2. These fixed novel views are subsequently added to the training set to further supervise the 3DGS optimization in an iterative way.

Reference-guided Trajectory. Trajectory sampling is critical in this iterative optimization process. Common sampling strategies, such as interpolation trajectory between input poses (Figure 3 (a)) or ellipse trajectory along a spherical path across all the camera poses (Figure 3 (b)), have limitations. For our GSFixer, The interpolation trajectory yields high-quality fixed novel views but lacks angular diversity, while the ellipse trajectory provides broader view coverage but results in suboptimal fixed views. To balance these trade-offs, we propose a reference-guided trajectory sampling strategy, as shown in Figure 3 (c). Specifically, (i) we first interpolate from a reference view to its nearest viewpoint on the spherical path, (ii) sample additional views along the sphere path, (iii) and then interpolate to the next nearest reference view. This hybrid sampling strategy achieves high-quality fixed views and angle coverage, leading to better 3DGS representation.

During optimization, we freeze the video diffusion model and supervise the 3DGS representation using a loss function \mathcal{L} composed of two components: the reconstruction loss \mathcal{L}_{recon} between rendered images and the input sparse views, and the generative loss \mathcal{L}_{gen} between the rendered novel views and the corresponding fixed novel views. Specifically, we adopt simple photometric losses:

$$\mathcal{L}_{recon} = \lambda_{l1} \cdot \mathcal{L}_{l1} + \lambda_{SSIM} \cdot \mathcal{L}_{SSIM}. \quad (8)$$

	PSNR \uparrow	SSIM \uparrow	LPIPS \downarrow	I2V_SC \uparrow	I2V_BC \uparrow	OC \uparrow	TF \uparrow	MS \uparrow
Artifact (Kerbl et al., 2023)	14.12	0.405	0.509	0.9382	0.9524	0.2066	0.9058	0.9548
Difix3D+ (Wu et al., 2025a)	14.14	0.419	0.455	0.9288	0.9481	0.2393	0.9038	0.9473
GenFusion (Wu et al., 2025b)	14.56	0.453	0.486	0.8916	0.9258	0.2372	0.9135	0.9596
GSFixer (Ours)	16.72	0.520	0.399	0.9553	0.9644	0.2407	0.9233	0.9665

Table 1: **Quantitative comparison on DL3DV-Res Dataset.** We compare the video 3D artifact restoration results with baselines. The best results are highlighted in **bold**.

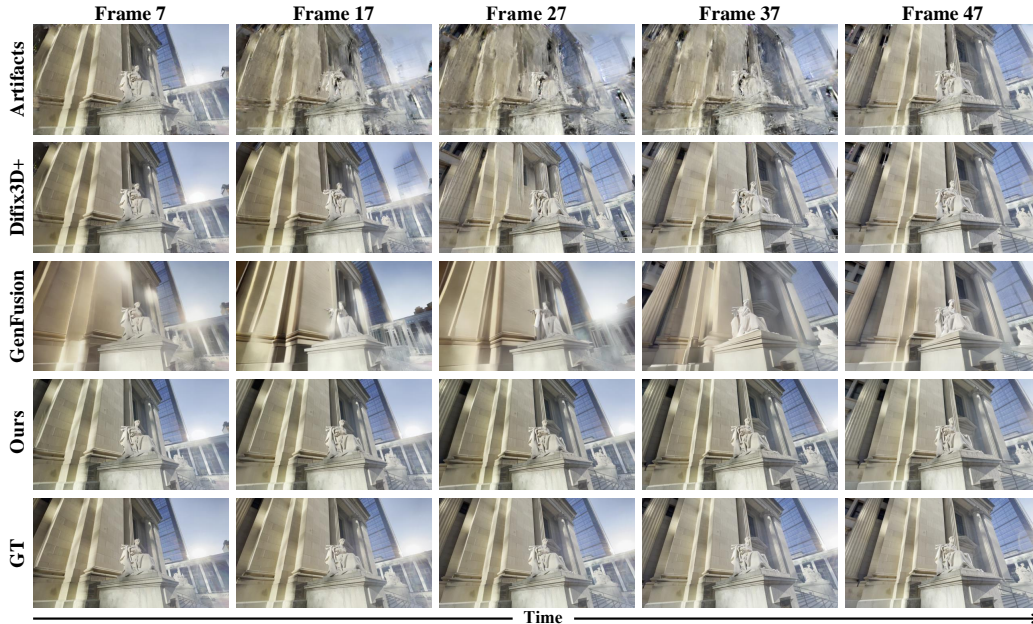


Figure 4: **Qualitative comparison on DL3DV-Res Benchmark.** We compare 3DGS artifact restoration quality of the existing generative methods.

The generative loss \mathcal{L}_{gen} consists of the same components as \mathcal{L}_{recon} but is applied to the rendered and fixed novel views:

$$\mathcal{L} = \mathcal{L}_{recon} + \lambda \cdot \mathcal{L}_{gen}, \quad (9)$$

where we employ an annealing strategy Wu et al. (2025b) to gradually increase the weight of the generative loss λ during training.

4 EXPERIMENTS

4.1 EXPERIMENTAL SETUP

Training Dataset and Evaluation Benchmarks. We train our GSFixer on a random selection of 1,000 scenes from the DL3DV-10K dataset (Ling et al., 2024). To construct paired artifact-laden and clean 3DGS renders, we employ a sparse-view 3D reconstruction strategy. Specifically, we use a few of input views (e.g., 3, 6, or 9) to reconstruct low-quality 3DGS representations. We then select camera trajectories from the dataset that include both the input views (used as reference views) and novel viewpoints (serving as ground truth frames). By rendering the low-quality 3DGS along these trajectories, we can generate the corresponding artifact-containing frames. Additionally, we extract the 1D text captions, 2D semantic tokens and 3D geometric tokens of the reference views by the pretrained BLIP, DINOv2 and VGGT encoders, respectively.

We evaluate our method and other baselines on 137 scenes from our proposed DL3DV-Res benchmark for the 3DGS artifact restoration task, and 28 scenes from the DL3DV-Benchmark (Ling et al., 2024) and 9 scenes from the Mip-NeRF 360 dataset (Barron et al., 2022) for the sparse-view 3D reconstruction task. For evaluation, we report PSNR, SSIM, and LPIPS metrics and Overall Consis-

	PSNR \uparrow			SSIM \uparrow			LPIPS \downarrow		
	3-view	6-view	9-view	3-view	6-view	9-view	3-view	6-view	9-view
3DGS (Kerbl et al., 2023)	13.72	17.11	19.05	0.410	0.547	0.625	0.521	0.372	0.293
Difix3D+ (Wu et al., 2025a)	15.07	18.26	20.12	0.481	0.589	0.656	0.473	0.329	0.259
GenFusion (Wu et al., 2025b)	14.64	18.36	20.32	0.498	0.610	0.688	0.493	0.374	0.314
GSFixer (Ours)	16.21	19.11	20.60	0.536	0.625	0.675	0.478	0.360	0.307

Table 2: **Quantitative comparison on DL3DV-Benchmark Dataset.** We compare the rendering quality with baselines given 3, 6 and 9 views.

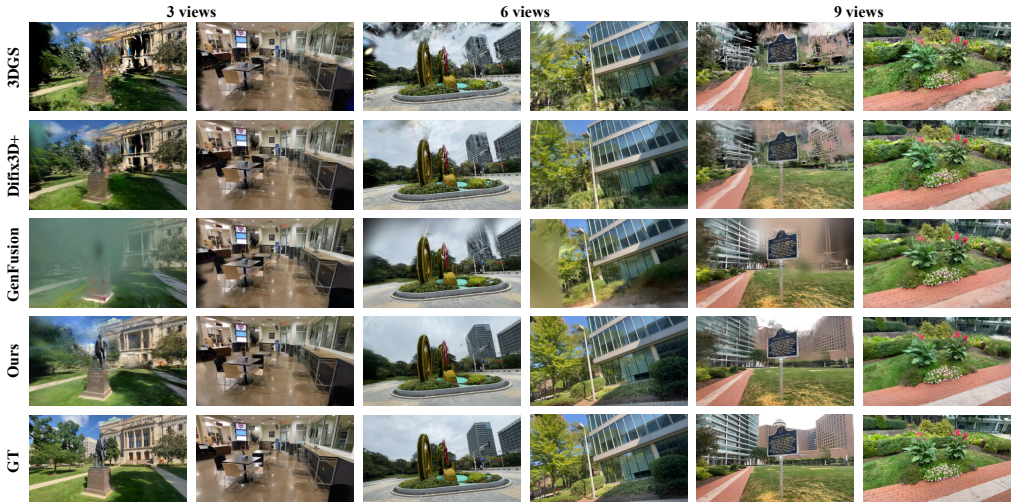


Figure 5: **Qualitative comparison on DL3DV-Benchmark.** We compare the novel view with baselines rendering quality using 3, 6, and 9 input views.

tency (OC), Temporal Flickering (TF), Motion Smoothness (MS) scores of VBench (Huang et al., 2024b) and I2V_Subject Consistency (I2V_SC), I2V_Background Consistency (I2V_BC) scores of VBench++ (Huang et al., 2024c) protocol.

The DL3DV-Res benchmark is constructed from all available scenes in the DL3DV-Benchmark, using a similar sparse-view reconstruction protocol. We train 3DGS models with extremely sparse input views (e.g., 3) and render the reconstructions along the original camera trajectories of each scene. This produces novel views with severe artifacts, paired with high-quality ground truth images. For fair comparison, all the methods initialize with the COLMAP (Schonberger & Frahm, 2016) point cloud in all the experiments and we filter and retain only the visible points from the input sparse training views.

Implementation Details. We implement and initialize the parameters of our reference-guided video diffusion model based on the pretrained CogVideoX-5B-I2V (Yang et al., 2024). During training, the frame resolution is fixed at 480×720 , and the video length is set to 49 frames. The training stage is conducted for 10,000 iterations with a learning rate of 2×10^{-5} , incorporating a warm-up strategy, and optimized using the AdamW optimizer. The proposed model is trained on 8 NVIDIA H20 GPUs with a batch size of 8 for about 4 days.

4.2 COMPARISON WITH OTHER METHODS

3DGS Artifact Restoration. To evaluate the effectiveness of existing models in 3DGS artifact restoration, we compare our GSFixer with recent generative methods, including Difix3D+ (Wu et al., 2025a) and GenFusion (Wu et al., 2025b) on our proposed DL3DV-Res benchmark. As shown in Table 1, the quantitative results demonstrate that GSFixer significantly outperforms both Difix3D+ and GenFusion in correcting artifacts in novel views across all pixel-wise metrics. Specifically, GSFixer achieves improvements of 2.16 in PSNR, 0.067 in SSIM, and 0.087 in LPIPS compared to GenFusion. Furthermore, our method consistently outperforms the baselines across all VBench and VBench++ metrics, showcasing state-of-the-art performance in 3DGS artifact restoration. It is

	PSNR \uparrow			SSIM \uparrow			LPIPS \downarrow		
	3-view	6-view	9-view	3-view	6-view	9-view	3-view	6-view	9-view
Zip-NeRF [†] (Barron et al., 2023)	12.77	13.61	14.30	0.271	0.284	0.312	0.705	0.663	0.633
FreeNeRF [†] (Yang et al., 2023)	12.87	13.35	14.59	0.260	0.283	0.319	0.715	0.717	0.695
SimpleNeRF [†] (Somraj et al., 2023)	13.27	13.67	15.15	0.283	0.312	0.354	0.741	0.721	0.676
ZeroNVS [†] (Sargent et al., 2024)	14.44	15.51	15.99	0.316	0.337	0.350	0.680	0.663	0.655
ReconFusion [†] (Wu et al., 2024)	15.50	16.93	18.19	0.358	0.401	0.432	0.585	0.544	0.511
3DGS [†] (Kerbl et al., 2023)	13.06	14.96	16.79	0.251	0.355	0.447	0.576	0.505	0.446
2DGS [†] (Huang et al., 2024a)	13.07	15.02	16.67	0.243	0.338	0.423	0.580	0.506	0.449
FSGS [†] (Zhu et al., 2024)	14.17	16.12	17.94	0.318	0.415	0.492	0.578	0.517	0.468
Difix3D+ [‡] (Wu et al., 2025a)	13.92	15.94	17.54	0.298	0.382	0.452	0.578	0.468	0.391
GenFusion [‡] (Wu et al., 2025b)	15.03	16.90	18.29	0.357	0.430	0.489	0.578	0.494	0.440
GSFixer (Ours)	15.61	17.27	18.63	0.370	0.426	0.481	0.559	0.478	0.420

Table 3: **Quantitative Comparison on Mip-NeRF 360 Dataset.** We compare the rendering quality with baselines given 3, 6 and 9 views. [†] denotes results reproduced by ReconFusion and GenFusion, while [‡] indicates results reproduced by us on their official implementation.



Figure 6: **Qualitative comparison on Mip-NeRF 360.** We compare the novel view rendering quality with baselines using 3, 6, and 9 input views.

noteworthy that the I2V_SC and I2V_BC scores of Difix3D+ and GenFusion are even lower than the original artifact frames after their artifact correction, suggesting that these methods struggle to maintain consistency when fixing artifacts in novel views. The qualitative comparisons in Figure 4 further emphasize GSFixer’s superior quality and consistency in fixing the artifacts of novel views. For instance, Difix3D+ and GenFusion fail to restore the content consistently, such as the foreground statue and background buildings. See supplement for more details.

In Domain Sparse View Reconstruction. We next compare our method with baseline approaches for sparse-view 3D reconstruction on the DL3DV-Benchmark. As shown in Table 2 and Figure 5, our GSFixer achieves more realistic novel view synthesis across 3, 6, and 9 input views. For example, under the extremely sparse 3-view setting, GSFixer significantly improves 3DGS quality by 3.55 dB in PSNR, 0.119 in SSIM, and 0.034 in LPIPS. Moreover, our GSFixer outperforms state-of-the-art methods such as Difix3D+ and GenFusion by a substantial margin. Difix3D+ fails to generate plausible content in occluded or missing regions, as illustrated in the building structure in the first row of the figure. It also does not adequately fix geometry-distorted Gaussians, as seen in the road reconstruction in the fifth and sixth rows. Additionally, inconsistent novel views generated by Difix3D+’s image diffusion process degrade overall quality, particularly noticeable in the statue (first row) and in the building and sky regions (third row). Similarly, GenFusion exhibits notable artifacts in fixing 3DGS representation. For example, its video diffusion process generates “foggy”

	PSNR \uparrow	SSIM \uparrow	LPIPS \downarrow	I2V_SC \uparrow	I2V_BC \uparrow	OC \uparrow	TF \uparrow	MS \uparrow
Ours w/o 3D tokens	16.36	0.510	0.414	0.9527	0.9630	0.2403	0.9218	0.9663
Ours w/o 2D tokens	16.48	0.516	0.409	0.9540	0.9635	0.2405	0.9225	0.9665
Ours full model	16.72	0.520	0.399	0.9553	0.9644	0.2407	0.9233	0.9665

Table 4: **Ablation study about different conditions.** We report the PSNR, SSIM, LPIPS, VBench and VBench++ metrics for the full model and its ablated versions on DL3DV-Res.

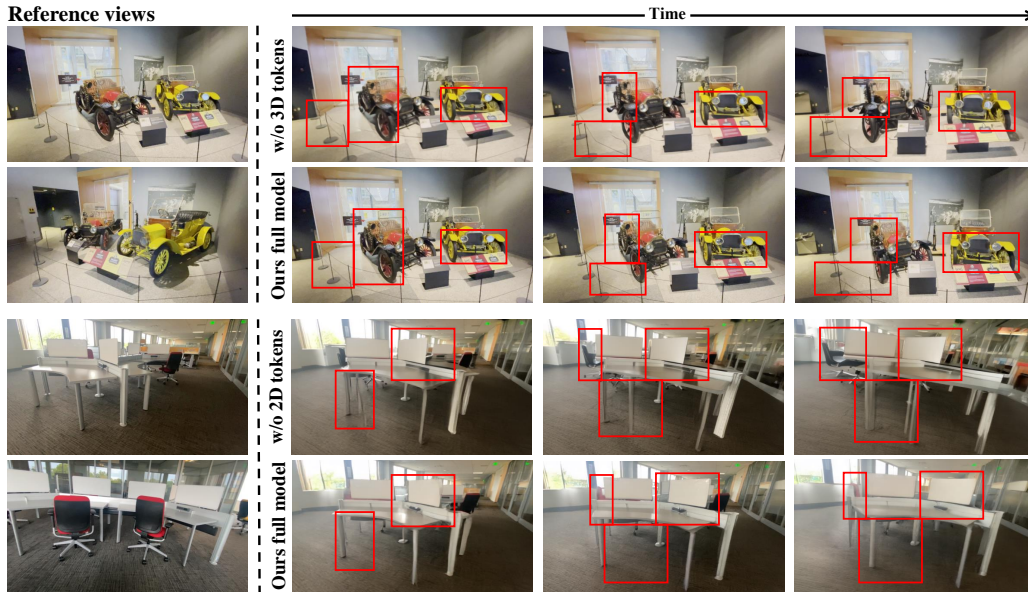


Figure 7: **Effectiveness of reference view conditions.** We compare our full model with two alternatives: a variant without 3D conditions (top), and a variant without 2D conditions (bottom). The red boxes highlight the most prominent differences.

geometry in the background (statue in first row and building in fifth row), failing to produce 3D-consistent content in missing regions. This results in blurred renderings, as shown in the third and fourth rows. In contrast, our GSFixer effectively inpaints plausible content in missing regions and performs both semantically and geometrically consistent fixes in novel views, leading to high-quality and coherent novel view renderings.

Out of Domain Sparse View Reconstruction. To demonstrate the generalizability of our method for out-of-distribution dataset, we further evaluate the methods on the challenging Mip-NeRF 360 dataset with 3, 6, and 9 input views. The quantitative results presented in Table 5 show that our GSFixer outperforms the baseline approaches, highlighting its strong generalization performance on unseen and complex scenes. For instance, our GSFixer surpasses generative 3DGS-based methods such as Diffix3D+ and GenFusion. Moreover, we observe that our GSFixer even outperforms generative NeRF-based ReconFusion in sparse view settings. This is particularly notable as 3DGS is generally more prone to overfitting on sparse input views compared to NeRF. Qualitative results shown in Figure 6 further illustrate the semantic and 3D consistent generative capability of our GSFixer. For detailed per-scene results, please refer to the supplementary material.

4.3 ABLATION STUDIES

Effectiveness of Reference View Conditions. We conduct an ablation study on one of our key contributions: the reference-guided video restoration model, which controls the 3DGS artifact restoration process using 3D and 2D tokens extracted from reference views. We compare the video restoration results of three variants on the DL3DV-Res benchmark: our full model, a version without 3D tokens, and one without 2D tokens. As quantitatively results presented in Table 4, our full model consistently outperforms the other two variants across all metrics. The qualitative comparisons in Figure 7 further support this finding. From the visualization, we observe that removing the 3D

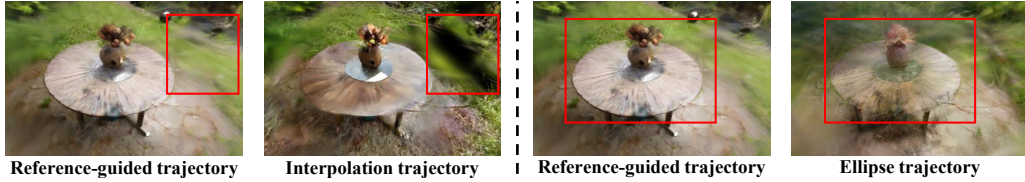


Figure 8: **Effectiveness of reference-guided trajectory.** We compare with widely used interpolation trajectory and ellipse trajectory. The red boxes highlight the most prominent differences.

	PSNR \uparrow	SSIM \uparrow	LPIPS \downarrow
Interpolation trajectory	14.50	0.353	0.565
Ellipse trajectory	15.46	0.362	0.563
Reference-guided trajectory	15.61	0.370	0.559

Table 5: **Ablation study about trajectory sampling.** We report the PSNR, SSIM, and LPIPS metrics for different trajectories on Mip-NeRF 360.

condition leads to poor 3D consistency with the reference views, e.g., misalignment in the fence and cars (highlighted in red boxes). This is because 3DGS renders under sparse-view settings often exhibit severe geometric distortions, making it difficult for the diffusion model to generate geometrically consistent content without strong 3D priors. Similarly, without the 2D condition, the model fails to restore semantically plausible details, such as the table leg, baffle, socket, and chair marked in red boxes. In contrast, our full model successfully restores artifact-ridden novel views to frames that are both 3D-consistent and semantically aligned with the reference views, demonstrating the effectiveness of injecting both 3D and 2D conditions into the video diffusion model.

Effectiveness of Reference Guided Trajectory. To validate the effectiveness of our reference-guided-trajectory sampling strategy, we further conduct an ablation study on the challenging Mip-NeRF 360 dataset using a 3-view 3D reconstruction setting. Qualitative results are presented in Figure 8, with the most notable differences highlighted in red boxes. As shown in the figure, the interpolation trajectory lacks sufficient angular coverage, leading to incomplete reconstructions with missing regions. Meanwhile, the ellipse trajectory results in degraded rendering quality, as the novel views to be restored are not temporally sequential with the reference views. In contrast, our reference-guided trajectory ensures both coverage and quality in the reconstruction process. The quantitative results in Table 5 further confirm the effectiveness of the reference-guided trajectory sampling strategy.

5 CONCLUSIONS

We present GSFixer, a novel pipeline for enhancing the quality of 3D Gaussian Splatting in sparse-view 3D reconstruction and novel view synthesis. Our reference-guided video restoration model integrates both 3D geometric and 2D semantic condition signals from reference views, ensuring semantically coherent and geometrically consistent artifact correction in novel views. Furthermore, we introduce a reference-guided trajectory sampling strategy within the iterative reconstruction process, enabling high-quality 3D reconstruction. In addition, we propose the DL3DV-Res benchmark to evaluate the 3DGS artifact restoration capability.

Limitations and Future Work. Our GSFixer builds upon a DiT-based video diffusion model that requires 50 denoising steps, which may limit the efficiency. As a 3D enhancement model, its performance is inherently limited by the quality of the initial 3DGS representation. Future work may explore improving GSFixer with advanced single-step video diffusion models and improved 3D representation, enabling efficient and high-fidelity novel view synthesis.

REFERENCES

- Chong Bao, Xiyu Zhang, Zehao Yu, Jiale Shi, Guofeng Zhang, Songyou Peng, and Zhaopeng Cui. Free360: Layered gaussian splatting for unbounded 360-degree view synthesis from extremely sparse and unposed views. In *Proceedings of the Computer Vision and Pattern Recognition Conference*, pp. 16377–16387, 2025.
- Jonathan T Barron, Ben Mildenhall, Dor Verbin, Pratul P Srinivasan, and Peter Hedman. Mip-nerf 360: Unbounded anti-aliased neural radiance fields. In *Proceedings of the IEEE/CVF Conference on Computer Vision and Pattern Recognition*, pp. 5470–5479, 2022.
- Jonathan T Barron, Ben Mildenhall, Dor Verbin, Pratul P Srinivasan, and Peter Hedman. Zip-nerf: Anti-aliased grid-based neural radiance fields. In *Proceedings of the IEEE/CVF International Conference on Computer Vision*, pp. 19697–19705, 2023.
- Andreas Blattmann, Tim Dockhorn, Sumith Kulal, Daniel Mendelevitch, Maciej Kilian, Dominik Lorenz, Yam Levi, Zion English, Vikram Voleti, Adam Letts, et al. Stable video diffusion: Scaling latent video diffusion models to large datasets. *arXiv preprint arXiv:2311.15127*, 2023.
- Tim Brooks, Bill Peebles, Connor Holmes, Will DePue, Yufei Guo, Li Jing, David Schnurr, Joe Taylor, Troy Luhman, Eric Luhman, et al. Video generation models as world simulators. 2024.
- Haoxin Chen, Menghan Xia, Yingqing He, Yong Zhang, Xiaodong Cun, Shaoshu Yang, Jinbo Xing, Yaofang Liu, Qifeng Chen, Xintao Wang, et al. Videocrafter1: Open diffusion models for high-quality video generation. *arXiv preprint arXiv:2310.19512*, 2023.
- Haoxin Chen, Yong Zhang, Xiaodong Cun, Menghan Xia, Xintao Wang, Chao Weng, and Ying Shan. Videocrafter2: Overcoming data limitations for high-quality video diffusion models. In *Proceedings of the IEEE/CVF Conference on Computer Vision and Pattern Recognition*, pp. 7310–7320, 2024.
- Jiahao Cui, Hui Li, Yun Zhan, Hanlin Shang, Kaihui Cheng, Yuqi Ma, Shan Mu, Hang Zhou, Jingdong Wang, and Siyu Zhu. Hallo3: Highly dynamic and realistic portrait image animation with video diffusion transformer. In *Proceedings of the Computer Vision and Pattern Recognition Conference*, pp. 21086–21095, 2025.
- Kangle Deng, Andrew Liu, Jun-Yan Zhu, and Deva Ramanan. Depth-supervised nerf: Fewer views and faster training for free. In *Proceedings of the IEEE/CVF Conference on Computer Vision and Pattern Recognition*, pp. 12882–12891, 2022.
- Zekai Gu, Rui Yan, Jiahao Lu, Peng Li, Zhiyang Dou, Chenyang Si, Zhen Dong, Qifeng Liu, Cheng Lin, Ziwei Liu, et al. Diffusion as shader: 3d-aware video diffusion for versatile video generation control. In *SIGGRAPH*, 2025.
- Ayaan Haque, Matthew Tancik, Alexei A Efros, Aleksander Holynski, and Angjoo Kanazawa. Instruct-nerf2nerf: Editing 3d scenes with instructions. In *Proceedings of the IEEE/CVF International Conference on Computer Vision*, pp. 19740–19750, 2023.
- Hao He, Yinghao Xu, Yuwei Guo, Gordon Wetzstein, Bo Dai, Hongsheng Li, and Ceyuan Yang. Cameractrl: Enabling camera control for video diffusion models. In *International Conference on Learning Representations*, 2025.
- Li Hu. Animate anyone: Consistent and controllable image-to-video synthesis for character animation. In *Proceedings of the IEEE/CVF Conference on Computer Vision and Pattern Recognition*, pp. 8153–8163, 2024.
- Wenbo Hu, Xiangjun Gao, Xiaoyu Li, Sijie Zhao, Xiaodong Cun, Yong Zhang, Long Quan, and Ying Shan. Depthcrafter: Generating consistent long depth sequences for open-world videos. In *Proceedings of the Computer Vision and Pattern Recognition Conference*, pp. 2005–2015, 2025.
- Binbin Huang, Zehao Yu, Anpei Chen, Andreas Geiger, and Shenghua Gao. 2d gaussian splatting for geometrically accurate radiance fields. In *SIGGRAPH 2024*, pp. 1–11, 2024a.

-
- Ziqi Huang, Yanan He, Jiashuo Yu, Fan Zhang, Chenyang Si, Yuming Jiang, Yuanhan Zhang, Tianxing Wu, Qingyang Jin, Nattapol Chanpaisit, et al. Vbench: Comprehensive benchmark suite for video generative models. In *Proceedings of the IEEE/CVF Conference on Computer Vision and Pattern Recognition*, pp. 21807–21818, 2024b.
- Ziqi Huang, Fan Zhang, Xiaojie Xu, Yanan He, Jiashuo Yu, Ziyue Dong, Qianli Ma, Nattapol Chanpaisit, Chenyang Si, Yuming Jiang, et al. Vbench++: Comprehensive and versatile benchmark suite for video generative models. *arXiv preprint arXiv:2411.13503*, 2024c.
- Ajay Jain, Matthew Tancik, and Pieter Abbeel. Putting nerf on a diet: Semantically consistent few-shot view synthesis. In *Proceedings of the IEEE/CVF International Conference on Computer Vision*, pp. 5885–5894, 2021.
- Bernhard Kerbl, Georgios Kopanas, Thomas Leimkühler, and George Drettakis. 3d gaussian splatting for real-time radiance field rendering. *ACM Transactions on Graphics*, pp. 139–1, 2023.
- Zhe Kong, Feng Gao, Yong Zhang, Zhuoliang Kang, Xiaoming Wei, Xunliang Cai, Guanying Chen, and Wenhan Luo. Let them talk: Audio-driven multi-person conversational video generation. *arXiv preprint arXiv:2505.22647*, 2025.
- Jiahe Li, Jiawei Zhang, Xiao Bai, Jin Zheng, Xin Ning, Jun Zhou, and Lin Gu. Dngaussian: Optimizing sparse-view 3d gaussian radiance fields with global-local depth normalization. In *Proceedings of the IEEE/CVF Conference on Computer Vision and Pattern Recognition*, pp. 20775–20785, 2024.
- Junnan Li, Dongxu Li, Caiming Xiong, and Steven Hoi. Blip: Bootstrapping language-image pre-training for unified vision-language understanding and generation. In *International Conference on Machine Learning*, pp. 12888–12900, 2022.
- Lu Ling, Yichen Sheng, Zhi Tu, Wentian Zhao, Cheng Xin, Kun Wan, Lantao Yu, Qianyu Guo, Zixun Yu, Yawen Lu, et al. D13dv-10k: A large-scale scene dataset for deep learning-based 3d vision. In *Proceedings of the IEEE/CVF Conference on Computer Vision and Pattern Recognition*, pp. 22160–22169, 2024.
- Fangfu Liu, Wenqiang Sun, Hanyang Wang, Yikai Wang, Haowen Sun, Junliang Ye, Jun Zhang, and Yueqi Duan. Reconx: Reconstruct any scene from sparse views with video diffusion model. *arXiv preprint arXiv:2408.16767*, 2024a.
- Ruoshi Liu, Rundi Wu, Basile Van Hoorick, Pavel Tokmakov, Sergey Zakharov, and Carl Vondrick. Zero-1-to-3: Zero-shot one image to 3d object. In *Proceedings of the IEEE/CVF International Conference on Computer Vision*, pp. 9298–9309, 2023.
- Xi Liu, Chaoyi Zhou, and Siyu Huang. 3dgs-enhancer: Enhancing unbounded 3d gaussian splatting with view-consistent 2d diffusion priors. In *Advances in Neural Information Processing Systems*, pp. 133305–133327, 2024b.
- Ben Mildenhall, Pratul P Srinivasan, Matthew Tancik, Jonathan T Barron, Ravi Ramamoorthi, and Ren Ng. Nerf: Representing scenes as neural radiance fields for view synthesis. In *European Conference on Computer Vision*, pp. 405–421, 2020.
- Michael Niemeyer, Jonathan T Barron, Ben Mildenhall, Mehdi SM Sajjadi, Andreas Geiger, and Noha Radwan. Regnerf: Regularizing neural radiance fields for view synthesis from sparse inputs. In *Proceedings of the IEEE/CVF Conference on Computer Vision and Pattern Recognition*, pp. 5480–5490, 2022.
- Muyao Niu, Xiaodong Cun, Xintao Wang, Yong Zhang, Ying Shan, and Yinqiang Zheng. Mofa-video: Controllable image animation via generative motion field adaptations in frozen image-to-video diffusion model. In *European Conference on Computer Vision*, pp. 111–128, 2024.
- Maxime Oquab, Timothée Darcet, Théo Moutakanni, Huy Vo, Marc Szafraniec, Vasil Khalidov, Pierre Fernandez, Daniel Haziza, Francisco Massa, Alaaeldin El-Nouby, et al. DINOv2: Learning robust visual features without supervision. *Transactions on Machine Learning Research*, pp. 1–31, 2024.

-
- William Peebles and Saining Xie. Scalable diffusion models with transformers. In *Proceedings of the IEEE/CVF International Conference on Computer Vision*, pp. 4195–4205, 2023.
- Colin Raffel, Noam Shazeer, Adam Roberts, Katherine Lee, Sharan Narang, Michael Matena, Yanqi Zhou, Wei Li, and Peter J Liu. Exploring the limits of transfer learning with a unified text-to-text transformer. *Journal of Machine Learning Research*, pp. 1–67, 2020.
- Barbara Roessle, Jonathan T Barron, Ben Mildenhall, Pratul P Srinivasan, and Matthias Nießner. Dense depth priors for neural radiance fields from sparse input views. In *Proceedings of the IEEE/CVF Conference on Computer Vision and Pattern Recognition*, pp. 12892–12901, 2022.
- Robin Rombach, Andreas Blattmann, Dominik Lorenz, Patrick Esser, and Björn Ommer. High-resolution image synthesis with latent diffusion models. In *Proceedings of the IEEE/CVF Conference on Computer Vision and Pattern Recognition*, pp. 10684–10695, 2022.
- Kyle Sargent, Zizhang Li, Tanmay Shah, Charles Herrmann, Hong-Xing Yu, Yunzhi Zhang, Eric Ryan Chan, Dmitry Lagun, Li Fei-Fei, Deqing Sun, et al. Zeronvs: Zero-shot 360-degree view synthesis from a single image. In *Proceedings of the IEEE/CVF Conference on Computer Vision and Pattern Recognition*, pp. 9420–9429, 2024.
- Axel Sauer, Dominik Lorenz, Andreas Blattmann, and Robin Rombach. Adversarial diffusion distillation. In *European Conference on Computer Vision*, pp. 87–103, 2024.
- Johannes L Schonberger and Jan-Michael Frahm. Structure-from-motion revisited. In *Proceedings of the IEEE Conference on Computer Vision and Pattern Recognition*, pp. 4104–4113, 2016.
- Seunghyeon Seo, Yeonjin Chang, and Nojun Kwak. Flipnerf: Flipped reflection rays for few-shot novel view synthesis. In *Proceedings of the IEEE/CVF International Conference on Computer Vision*, pp. 22883–22893, 2023.
- Nagabhushan Somraj, Adithyan Karanayil, and Rajiv Soundararajan. Simplenerf: Regularizing sparse input neural radiance fields with simpler solutions. In *SIGGRAPH Asia*, pp. 1–11, 2023.
- Prune Truong, Marie-Julie Rakotosaona, Fabian Manhardt, and Federico Tombari. Sparf: Neural radiance fields from sparse and noisy poses. In *Proceedings of the IEEE/CVF Conference on Computer Vision and Pattern Recognition*, pp. 4190–4200, 2023.
- Team Wan, Ang Wang, Baole Ai, Bin Wen, Chaojie Mao, Chen-Wei Xie, Di Chen, Feiwu Yu, Haiming Zhao, Jianxiao Yang, et al. Wan: Open and advanced large-scale video generative models. *arXiv preprint arXiv:2503.20314*, 2025.
- Guangcong Wang, Zhaoxi Chen, Chen Change Loy, and Ziwei Liu. Sparsenerf: Distilling depth ranking for few-shot novel view synthesis. In *Proceedings of the IEEE/CVF International Conference on Computer Vision*, pp. 9065–9076, 2023.
- Jianyuan Wang, Minghao Chen, Nikita Karaev, Andrea Vedaldi, Christian Rupprecht, and David Novotny. Vggt: Visual geometry grounded transformer. In *Proceedings of the Computer Vision and Pattern Recognition Conference*, pp. 5294–5306, 2025.
- Zhouxia Wang, Ziyang Yuan, Xintao Wang, Yaowei Li, Tianshui Chen, Menghan Xia, Ping Luo, and Ying Shan. Motionctrl: A unified and flexible motion controller for video generation. In *ACM SIGGRAPH*, pp. 1–11, 2024.
- Jay Zhangjie Wu, Yuxuan Zhang, Haithem Turki, Xuanchi Ren, Jun Gao, Mike Zheng Shou, Sanja Fidler, Zan Gojcic, and Huan Ling. Difix3d+: Improving 3d reconstructions with single-step diffusion models. In *Proceedings of the Computer Vision and Pattern Recognition Conference*, pp. 26024–26035, 2025a.
- Rundi Wu, Ben Mildenhall, Philipp Henzler, Keunhong Park, Ruiqi Gao, Daniel Watson, Pratul P Srinivasan, Dor Verbin, Jonathan T Barron, Ben Poole, et al. Reconfusion: 3d reconstruction with diffusion priors. In *Proceedings of the IEEE/CVF Conference on Computer Vision and Pattern Recognition*, pp. 21551–21561, 2024.

-
- Sibo Wu, Congrong Xu, Binbin Huang, Andreas Geiger, and Anpei Chen. Genfusion: Closing the loop between reconstruction and generation via videos. In *Proceedings of the Computer Vision and Pattern Recognition Conference*, pp. 6078–6088, 2025b.
- Jinbo Xing, Menghan Xia, Yong Zhang, Haoxin Chen, Wangbo Yu, Hanyuan Liu, Gongye Liu, Xintao Wang, Ying Shan, and Tien-Tsin Wong. Dynamicrafter: Animating open-domain images with video diffusion priors. In *European Conference on Computer Vision*, pp. 399–417, 2024.
- Yexing Xu, Longguang Wang, Minglin Chen, Sheng Ao, Li Li, and Yulan Guo. Dropouts: Dropping out gaussians for better sparse-view rendering. In *Proceedings of the Computer Vision and Pattern Recognition Conference*, pp. 701–710, 2025.
- Jiawei Yang, Marco Pavone, and Yue Wang. Freenerf: Improving few-shot neural rendering with free frequency regularization. In *Proceedings of the IEEE/CVF Conference on Computer Vision and Pattern Recognition*, pp. 8254–8263, 2023.
- Zhuoyi Yang, Jiayan Teng, Wendi Zheng, Ming Ding, Shiyu Huang, Jiazheng Xu, Yuanming Yang, Wenyi Hong, Xiaohan Zhang, Guanyu Feng, et al. Cogvideox: Text-to-video diffusion models with an expert transformer. *arXiv preprint arXiv:2408.06072*, 2024.
- Alex Yu, Vickie Ye, Matthew Tancik, and Angjoo Kanazawa. pixelnerf: Neural radiance fields from one or few images. In *Proceedings of the IEEE/CVF Conference on Computer Vision and Pattern Recognition*, pp. 4578–4587, 2021.
- Mark YU, Wenbo Hu, Jinbo Xing, and Ying Shan. Trajectoryrafter: Redirecting camera trajectory for monocular videos via diffusion models. *arXiv preprint arXiv:2503.05638*, 2025.
- Wangbo Yu, Jinbo Xing, Li Yuan, Wenbo Hu, Xiaoyu Li, Zhipeng Huang, Xiangjun Gao, Tien-Tsin Wong, Ying Shan, and Yonghong Tian. Viewrafter: Taming video diffusion models for high-fidelity novel view synthesis. *arXiv preprint arXiv:2409.02048*, 2024.
- Zehao Yu, Songyou Peng, Michael Niemeyer, Torsten Sattler, and Andreas Geiger. Monosdf: Exploring monocular geometric cues for neural implicit surface reconstruction. In *Advances in Neural Information Processing Systems*, pp. 25018–25032, 2022.
- David Junhao Zhang, Roni Paiss, Shiran Zada, Nikhil Karnad, David E Jacobs, Yael Pritch, Inbar Mosseri, Mike Zheng Shou, Neal Wadhwa, and Nataniel Ruiz. Recapture: Generative video camera controls for user-provided videos using masked video fine-tuning. In *Proceedings of the Computer Vision and Pattern Recognition Conference*, pp. 2050–2062, 2025.
- Jiahui Zhang, Fangneng Zhan, Muyu Xu, Shijian Lu, and Eric Xing. Fregs: 3d gaussian splatting with progressive frequency regularization. In *Proceedings of the IEEE/CVF Conference on Computer Vision and Pattern Recognition*, pp. 21424–21433, 2024.
- Sijie Zhao, Wenbo Hu, Xiaodong Cun, Yong Zhang, Xiaoyu Li, Zhe Kong, Xiangjun Gao, Muyao Niu, and Ying Shan. Stereocrafter: Diffusion-based generation of long and high-fidelity stereoscopic 3d from monocular videos. *arXiv preprint arXiv:2409.07447*, 2024.
- Zehao Zhu, Zhiwen Fan, Yifan Jiang, and Zhangyang Wang. Fsgs: Real-time few-shot view synthesis using gaussian splatting. In *European Conference on Computer Vision*, pp. 145–163, 2024.

APPENDIX: GSFIXER: IMPROVING 3D GAUSSIAN SPLATTING VIA REFERENCE-GUIDED VIDEO DIFFUSION PRIORS

A REFERENCE-GUIDED VIDEO DIFFUSION MODEL DETAILS

Our reference-guided video diffusion model is built upon CogVideoX-5B-I2V, a pretrained DiT-based video diffusion model capable of generating 49-frame videos at a resolution 480×720 from a single input image. In our video-to-video restoration task, which aims to restore artifact frames into clean ones, we replace the original image condition with the 3DGS renders $\{I_n^{nov}\}_{n=1, \dots, 47}$ between two reference views $\{I_1, I_2\}$. In the training process, each training sample consists of a sequence of 47-frame artifact-prone 3DGS renders, two reference images, and 49-frame ground truth RGB video. The artifact frames ($49 \times 3 \times 480 \times 720$) and ground truth frames ($49 \times 3 \times 480 \times 720$) are first encoded into latent features using a 3DVAE, resulting in latent dimensions of $16 \times 13 \times 60 \times 90$. The ground truth latent features are then perturbed with noise for the diffusion training process. For the view tokens, we concatenate, patchify and project the latent features to 17550×3072 view tokens. For the text tokens, we use BLIP to generate text captions of the reference views and use T5 to extract 226×4096 feature embedding, which are projected to 226×3072 text tokens. To extract geometric and semantic conditioning signals, the two reference views are first resize to 350×518 to feed into VGGT and DINOv2 encoder to produce $2 \times 930 \times 2048$ geometric tokens and $2 \times 930 \times 1024$ semantic tokens. We abandon $2 \times 5 \times 2048$ camera token from VGGT, and remove $2 \times 1 \times 1024$ class token and $2 \times 4 \times 1024$ registration token from DINOv2, resulting in $2 \times 925 \times 2048$ 3D geometric tokens and $2 \times 925 \times 1024$ 2D semantic tokens. These are projected to $2 \times 925 \times 3072$ using $Projector_{3D}$ and $Projector_{2D}$, respectively. $Projector_{3D}$ is a linear layer mapping from 2048 to 3072 dimensions, followed by LayerNorm. $Projector_{2D}$ is a linear layer mapping from 1024 to 3072 dimensions, followed by LayerNorm. Finally, the 3D geometric and 2D semantic tokens are combined and reshaped into fusion tokens of dimension 1850×3072 , which serve as rich 3D and 2D priors to guide the restoration process of diffusion model. During inference, we employ DDIM sampling with classifier-free guidance to modulate condition adherence strength.

B DETAILS OF COMPARISON BASELINES

We compare our method with (i) regularization methods and (ii) generative methods for sparse-view reconstruction and 3DGS artifact restoration tasks. Specifically, we evaluate NeRF-based per-scene regularization methods including Zip-NeRF Barron et al. (2023), FreeNeRF Yang et al. (2023) and SimpleNeRF Somraj et al. (2023); NeRF-based generative methods such as ZeroNVS Sargent et al. (2024) and ReconFusion Wu et al. (2024); 3DGS-based per-scene regularization method FSGS Zhu et al. (2024); and 3DGS-based generative methods Difix3D+ Wu et al. (2025a) and GenFusion Wu et al. (2025b). Difix3D+ incorporates generative priors from the image diffusion model SD-turbo Sauer et al. (2024), finetuned on paired artifact renders and clean frames. In contrast, GenFusion bulids upon the video diffusion model DynamicCrafter Xing et al. (2024) that condition video frames on artifact-prone RGBD renders.

C MORE QUANTITATIVE AND QUALITATIVE RESULTS

We provide extensive per-scene experimental results in Figure 9, Table 6, Table 7, Table 8, Table 9, Table 10, and Table 11.

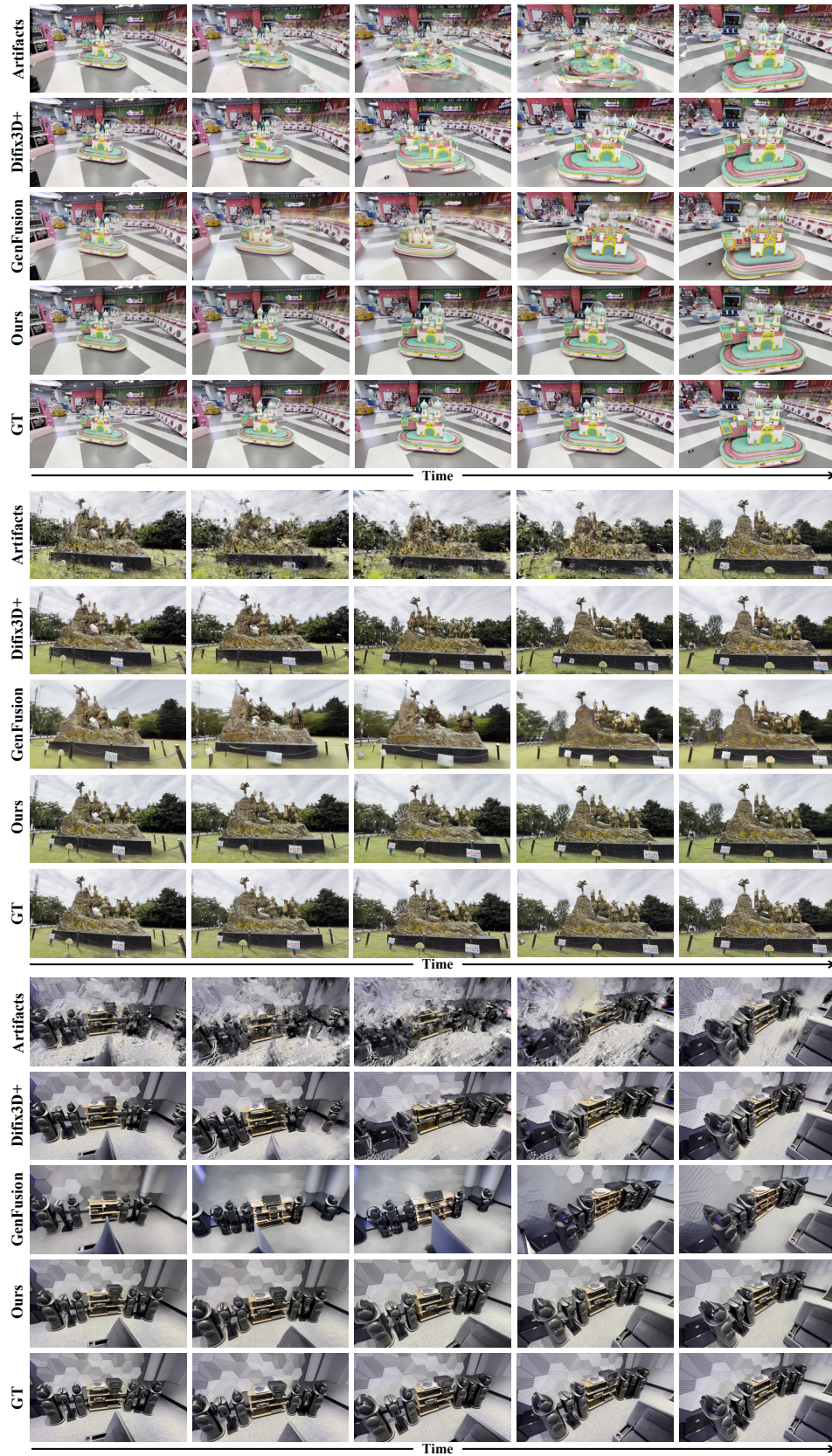


Figure 9: Qualitative comparison of 3DGS artifact restoration on DL3DV-Res.

	Artifact			Difix3D+			GenFusion			GSFixer (Ours)		
	PSNR↑	SSIM↑	LPIPS↓	PSNR↑	SSIM↑	LPIPS↓	PSNR↑	SSIM↑	LPIPS↓	PSNR↑	SSIM↑	LPIPS↓
032dee9fb0	17.43	0.510	0.447	17.04	0.521	0.375	17.03	0.573	0.412	23.07	0.709	0.196
0569e83fdc	12.65	0.218	0.567	12.42	0.214	0.536	12.79	0.250	0.562	15.32	0.330	0.458
06da796666	13.09	0.407	0.525	13.13	0.429	0.500	14.76	0.526	0.507	14.47	0.513	0.499
073f5a9b98	11.50	0.129	0.613	11.34	0.121	0.604	12.19	0.17	0.626	12.53	0.181	0.620
07d9f9724c	20.37	0.680	0.321	20.06	0.706	0.269	18.95	0.662	0.303	25.59	0.860	0.123
0853979305	17.24	0.530	0.442	17.33	0.549	0.391	17.55	0.578	0.419	19.51	0.625	0.355
093ef327b4	13.08	0.445	0.587	12.85	0.422	0.540	13.49	0.452	0.552	14.96	0.493	0.472
0a1b7c20a9	15.59	0.507	0.454	15.27	0.517	0.403	15.41	0.529	0.441	19.11	0.670	0.273
0a485338bb	15.13	0.467	0.466	15.24	0.491	0.402	15.89	0.491	0.440	20.23	0.623	0.290
0bfdd020cf	11.08	0.397	0.660	11.23	0.355	0.560	14.27	0.432	0.579	14.87	0.402	0.486
119fd56d37	12.41	0.331	0.599	12.45	0.360	0.563	13.13	0.452	0.563	13.93	0.468	0.552
1264931635	12.38	0.205	0.568	12.32	0.195	0.538	13.43	0.245	0.565	14.86	0.267	0.536
14eb48a50e	12.13	0.396	0.554	12.12	0.428	0.498	12.77	0.491	0.521	15.65	0.558	0.437
15ff83e253	13.37	0.360	0.576	13.59	0.330	0.491	14.00	0.389	0.552	15.65	0.383	0.474
165f5af8bf	14.59	0.374	0.492	14.87	0.396	0.420	15.47	0.429	0.462	16.86	0.477	0.384
183dd248f6	16.49	0.522	0.498	16.36	0.527	0.453	16.29	0.559	0.472	16.80	0.571	0.458
1ba74c2267	17.91	0.606	0.491	18.43	0.636	0.403	17.97	0.666	0.431	20.34	0.728	0.345
1d6a9ed47c	12.21	0.238	0.512	12.10	0.238	0.473	12.74	0.243	0.533	15.09	0.342	0.459
1da888bded	13.27	0.385	0.558	13.30	0.396	0.501	13.62	0.434	0.522	16.08	0.506	0.417
1de58be515	19.19	0.707	0.279	20.09	0.732	0.197	18.32	0.629	0.319	24.18	0.820	0.165
2385549d39	14.95	0.388	0.457	15.30	0.406	0.364	15.13	0.378	0.438	18.42	0.529	0.292
26fd23358f	14.40	0.353	0.510	14.19	0.371	0.448	14.33	0.385	0.495	17.60	0.484	0.363
286239bd0f	11.63	0.249	0.571	11.57	0.251	0.552	12.5	0.304	0.561	13.15	0.311	0.546
2991a75d1d	12.54	0.345	0.609	12.22	0.313	0.572	12.52	0.352	0.615	13.15	0.355	0.561
2b65ba886e	10.72	0.232	0.570	10.57	0.231	0.557	11.67	0.272	0.562	12.27	0.313	0.540
2beaca3189	12.30	0.268	0.580	11.99	0.271	0.541	12.74	0.305	0.570	14.58	0.373	0.465
2cbfe28643	16.33	0.559	0.425	16.98	0.606	0.314	16.49	0.595	0.395	20.11	0.725	0.231
2f3e1c0f68	13.57	0.380	0.519	13.67	0.409	0.462	14.28	0.475	0.482	15.83	0.511	0.421
32c2eb92fac	16.87	0.610	0.482	16.75	0.637	0.401	16.48	0.662	0.455	20.56	0.734	0.324
341b4ff3df	15.35	0.408	0.478	15.14	0.414	0.417	15.18	0.410	0.457	18.05	0.558	0.327
35317e6219	12.02	0.269	0.586	12.10	0.283	0.549	13.86	0.381	0.529	13.98	0.388	0.518
35872363e1	14.94	0.416	0.478	14.86	0.428	0.411	15.29	0.447	0.430	17.79	0.534	0.321
374ffd0c5f	18.72	0.569	0.418	19.11	0.604	0.337	17.99	0.614	0.394	21.89	0.723	0.247
387eeb925b	13.14	0.317	0.551	12.96	0.332	0.469	13.39	0.375	0.528	15.93	0.461	0.392
389a460ca1	13.66	0.523	0.502	13.58	0.545	0.435	12.75	0.556	0.503	15.08	0.619	0.432
3b16a10ec9	12.67	0.337	0.516	12.83	0.357	0.472	13.92	0.437	0.487	14.99	0.460	0.457
3b7529dccc	12.77	0.316	0.526	12.57	0.317	0.505	13.76	0.367	0.512	14.12	0.393	0.480
3bb3bb4d3e	14.81	0.561	0.458	14.92	0.594	0.393	16.06	0.658	0.375	18.12	0.710	0.297
3bb894d193	15.94	0.429	0.426	15.92	0.449	0.330	16.57	0.463	0.380	17.93	0.573	0.255
41036716da	14.98	0.473	0.502	15.13	0.508	0.441	15.00	0.525	0.466	16.99	0.593	0.376
444da1b4a3	12.16	0.347	0.515	11.84	0.365	0.468	11.85	0.377	0.486	16.33	0.564	0.310
457e9a1ae7	14.08	0.434	0.520	13.90	0.455	0.474	14.28	0.495	0.508	16.21	0.579	0.425
484c0aca40	13.87	0.504	0.492	13.71	0.536	0.429	13.86	0.565	0.472	16.33	0.663	0.348
493816813d	12.17	0.232	0.563	12.18	0.207	0.529	13.65	0.262	0.537	14.82	0.282	0.526
4ae797d07b	13.07	0.378	0.520	12.80	0.361	0.491	13.24	0.386	0.504	15.26	0.435	0.449
4ff8650b5c	14.93	0.470	0.499	14.84	0.488	0.457	14.87	0.518	0.476	16.16	0.559	0.404
50c46cf8b8	15.72	0.520	0.502	15.74	0.554	0.459	15.75	0.604	0.478	17.55	0.640	0.406
513e4ea2e8	14.46	0.417	0.502	14.62	0.438	0.424	14.38	0.455	0.487	20.25	0.644	0.227
54bf355ca7	13.61	0.380	0.524	13.51	0.384	0.496	14.33	0.441	0.505	15.20	0.459	0.469
56452d9cd9	14.39	0.328	0.517	14.58	0.345	0.470	15.28	0.396	0.501	16.41	0.421	0.453
565553aa89	13.51	0.318	0.527	13.65	0.338	0.474	14.67	0.384	0.487	16.35	0.453	0.408
599ca3e04c	14.48	0.453	0.525	14.22	0.473	0.477	13.87	0.478	0.485	15.53	0.532	0.448
5a27c00f52	13.64	0.384	0.470	13.40	0.391	0.400	13.75	0.395	0.437	17.23	0.547	0.286
5a69d1027b	10.68	0.192	0.661	10.83	0.168	0.604	13.23	0.262	0.629	13.42	0.240	0.568
5c3af58102	17.45	0.563	0.389	17.94	0.618	0.280	17.04	0.592	0.338	22.53	0.767	0.180
5f0041e53d	18.02	0.612	0.347	18.24	0.627	0.274	17.51	0.592	0.356	21.28	0.732	0.214
63798f5c6f	14.65	0.518	0.500	14.75	0.563	0.418	15.02	0.587	0.457	18.39	0.696	0.337
669c36225b	12.39	0.370	0.530	12.20	0.390	0.490	12.70	0.445	0.500	15.46	0.543	0.384
66fd66cbed	13.83	0.536	0.492	13.90	0.570	0.423	13.90	0.602	0.446	15.85	0.654	0.378
6d22162561	12.44	0.352	0.573	12.52	0.365	0.529	13.47	0.445	0.543	14.42	0.474	0.468
6d81c5ab0d	15.33	0.496	0.459	15.48	0.522	0.385	15.29	0.524	0.430	18.51	0.613	0.322
6e11e7f4fe	17.59	0.714	0.472	17.93	0.731	0.404	18.92	0.779	0.415	18.49	0.760	0.377
70eac6ff18	13.67	0.398	0.480	13.38	0.403	0.423	13.22	0.387	0.479	16.16	0.529	0.348
71b2dc8a2a	17.08	0.613	0.454	17.34	0.651	0.367	17.50	0.673	0.373	20.64	0.762	0.238
75fbb4e673	13.76	0.362	0.524	13.48	0.369	0.469	13.94	0.398	0.504	16.10	0.466	0.406
7705a2edd0	14.24	0.400	0.559	14.90	0.435	0.482	16.32	0.564	0.513	17.47	0.576	0.467
7a9f97660b	15.45	0.473	0.512	15.48	0.520	0.425	15.12	0.549	0.474	18.36	0.612	0.348
7da3db9905	12.92	0.450	0.521	12.83	0.455	0.477	13.48	0.472	0.494	13.78	0.504	0.467
800cf88687	13.75	0.318	0.524	13.42	0.321	0.490	13.67	0.350	0.518	15.43	0.376	0.467
8324b3ca22	12.22	0.304	0.592	12.35	0.327	0.548	13.04	0.417	0.551	13.76	0.410	0.522
85cd0e9211	14.24	0.365	0.528	14.40	0.386	0.469	14.28	0.432	0.498	16.48	0.472	0.429
8b9fb9d9f1	13.16	0.288	0.551	13.26	0.299	0.520	13.63	0.342	0.576	15.26	0.381	0.499
8cb2e97d26	14.88	0.382	0.521	14.90	0.404	0.424	14.38	0.427	0.494	20.39	0.617	0.300
8fdc5130f0	15.44	0.496	0.448	15.33	0.511	0.387	15.13	0.532	0.420	17.94	0.616	0.318
90cb7ef953	15.69	0.500	0.493	15.44	0.519	0.448	15.52	0.551	0.461	15.70	0.547	0.463
917e9c8985	14.17	0.387	0.477	13.90	0.395	0.436	14.27	0.418	0.469	16.48	0.529	0.345

Table 6: Per-scene 3DGS artifact restoration quantitative comparison on DL3DV-Res (Part 1).

	Artifact			Difix3D+			GenFusion			GSFixer (Ours)		
	PSNR↑	SSIM↑	LPIPS↓	PSNR↑	SSIM↑	LPIPS↓	PSNR↑	SSIM↑	LPIPS↓	PSNR↑	SSIM↑	LPIPS↓
91afb9910b	13.96	0.409	0.515	13.86	0.415	0.480	15.08	0.483	0.490	16.52	0.504	0.437
946f49be73	15.67	0.454	0.436	16.25	0.473	0.337	16.06	0.484	0.385	18.61	0.574	0.287
9641a1ed79	15.73	0.523	0.506	16.07	0.561	0.432	15.29	0.562	0.489	17.48	0.626	0.391
9c8c0e0fad	10.43	0.246	0.697	10.36	0.200	0.635	11.78	0.267	0.669	13.96	0.262	0.569
9cbe554864	12.32	0.256	0.550	12.11	0.259	0.529	12.76	0.296	0.543	14.95	0.382	0.456
9e9a89ae6f	15.54	0.627	0.412	15.38	0.640	0.340	14.37	0.638	0.412	17.25	0.703	0.319
9fb0588ff0	14.06	0.390	0.435	14.09	0.407	0.343	14.69	0.401	0.389	18.59	0.613	0.265
a17a984ca9	12.76	0.338	0.524	12.63	0.351	0.489	12.90	0.375	0.517	13.24	0.395	0.473
a401469cb0	12.77	0.358	0.572	12.67	0.371	0.539	13.49	0.432	0.564	14.64	0.457	0.510
a62c330f54	11.94	0.317	0.572	11.81	0.332	0.550	13.27	0.414	0.555	13.86	0.428	0.528
a62f9a1c63	13.93	0.400	0.502	14.00	0.412	0.420	13.63	0.406	0.494	17.54	0.545	0.343
a726c1112a	12.30	0.463	0.530	13.11	0.510	0.481	14.38	0.606	0.481	14.36	0.592	0.490
adb95f29c1	14.73	0.394	0.508	15.19	0.398	0.470	15.82	0.481	0.508	17.92	0.504	0.444
adf35184a1	15.87	0.526	0.523	15.86	0.559	0.438	15.68	0.588	0.484	20.09	0.691	0.339
af0d7039e6	12.33	0.310	0.509	12.01	0.303	0.479	12.80	0.338	0.494	13.27	0.365	0.479
b2076bc723	11.04	0.267	0.593	10.76	0.274	0.585	11.83	0.332	0.582	12.61	0.400	0.529
b3bf9079b4	16.08	0.461	0.441	16.23	0.496	0.371	15.98	0.502	0.414	18.68	0.579	0.326
b4f53094fd	13.97	0.384	0.487	13.75	0.388	0.429	13.60	0.380	0.487	16.73	0.506	0.349
b5faa2a8ce	13.90	0.429	0.537	14.29	0.443	0.469	17.50	0.566	0.468	16.88	0.560	0.434
b6d1134cb0	11.97	0.256	0.559	11.74	0.262	0.524	12.31	0.274	0.562	12.71	0.303	0.511
b92b499c9b	18.20	0.705	0.348	19.01	0.744	0.243	20.26	0.787	0.255	22.30	0.842	0.171
ba55c875d2	17.50	0.612	0.394	17.57	0.633	0.312	17.87	0.653	0.333	20.59	0.721	0.248
c076929db6	17.44	0.608	0.373	18.14	0.630	0.291	18.54	0.640	0.295	23.28	0.738	0.196
c37109a55e	12.10	0.247	0.547	11.94	0.253	0.516	12.83	0.280	0.545	13.39	0.298	0.508
c37726ce77	13.50	0.287	0.537	13.30	0.289	0.479	14.13	0.342	0.508	14.81	0.377	0.453
c455899acf	16.43	0.539	0.465	16.11	0.533	0.417	16.31	0.569	0.438	15.94	0.555	0.437
cbd44beb04	14.85	0.433	0.498	14.64	0.450	0.442	14.32	0.455	0.511	18.03	0.588	0.341
cd08c0bdc3	17.30	0.530	0.413	17.85	0.555	0.324	17.08	0.545	0.411	20.60	0.655	0.290
cd9c981eeb	12.40	0.300	0.539	12.41	0.313	0.492	12.82	0.351	0.510	14.82	0.438	0.420
ceb252f5d4	12.86	0.401	0.529	12.66	0.419	0.496	13.04	0.467	0.528	14.87	0.521	0.445
d1b3a0b37a	13.59	0.374	0.538	13.36	0.367	0.508	14.65	0.404	0.523	13.70	0.382	0.531
d3812aad53	10.99	0.341	0.576	11.03	0.362	0.540	12.07	0.440	0.554	11.90	0.408	0.555
d3af8212ae	15.82	0.425	0.481	16.10	0.456	0.405	16.51	0.491	0.447	21.05	0.623	0.272
d4f4beba016	12.10	0.171	0.565	11.74	0.164	0.540	12.45	0.199	0.560	12.86	0.206	0.556
d8de66037b	13.47	0.320	0.520	13.12	0.321	0.492	13.70	0.376	0.503	14.60	0.395	0.456
d904ae2998	11.63	0.322	0.568	11.52	0.320	0.552	12.94	0.411	0.556	13.22	0.399	0.558
d9b6376623	12.74	0.315	0.570	12.89	0.320	0.535	13.57	0.380	0.559	14.71	0.408	0.503
d9f4c746e6	15.33	0.516	0.409	15.59	0.543	0.329	16.54	0.564	0.346	19.76	0.698	0.210
dac9796dd6	14.38	0.503	0.510	14.11	0.535	0.450	13.56	0.535	0.472	18.62	0.700	0.273
dafa9c7cbd	11.35	0.137	0.599	11.21	0.132	0.579	12.26	0.164	0.587	12.58	0.190	0.581
ddfcdcfdf02	12.63	0.293	0.557	12.28	0.297	0.514	12.66	0.310	0.553	14.55	0.401	0.450
ded5e4b46a	17.44	0.563	0.506	17.23	0.580	0.458	17.80	0.628	0.479	18.78	0.658	0.425
df04f58064	14.02	0.277	0.529	13.91	0.285	0.481	13.90	0.286	0.532	17.45	0.442	0.376
df29c22586	15.52	0.402	0.425	15.60	0.421	0.338	15.80	0.427	0.397	20.31	0.589	0.281
df4f9d9a0a	13.12	0.473	0.321	13.26	0.504	0.430	14.42	0.563	0.452	17.58	0.662	0.340
e5684b3292	13.90	0.415	0.545	13.93	0.447	0.497	13.25	0.506	0.537	15.40	0.550	0.453
e78f8cebd2	12.51	0.206	0.562	12.45	0.209	0.534	13.32	0.241	0.546	14.71	0.296	0.491
e8ce51b6ab	14.38	0.491	0.499	14.17	0.513	0.438	14.27	0.529	0.486	18.52	0.687	0.284
e9360e7a89	12.13	0.319	0.554	11.84	0.319	0.521	12.31	0.335	0.565	12.67	0.362	0.516
eb4cf52988	13.75	0.417	0.543	13.53	0.431	0.518	14.12	0.476	0.532	15.67	0.526	0.478
ec1e44d4dc	13.81	0.452	0.534	13.50	0.481	0.489	13.51	0.506	0.497	16.37	0.606	0.353
ec305787b7	13.68	0.476	0.484	13.77	0.509	0.415	14.16	0.569	0.389	14.99	0.575	0.375
ed16328235	14.50	0.214	0.549	15.04	0.217	0.500	15.89	0.277	0.551	17.07	0.293	0.483
ef59aac437	17.15	0.331	0.515	17.32	0.338	0.443	17.71	0.381	0.498	19.97	0.465	0.361
f004c810d9	14.48	0.594	0.405	14.51	0.624	0.317	14.21	0.631	0.343	19.79	0.760	0.210
f477ffc4b3	14.75	0.528	0.490	14.38	0.551	0.421	13.7	0.534	0.461	17.21	0.635	0.336
f71ac346cd	13.23	0.230	0.534	13.06	0.224	0.499	13.72	0.254	0.529	15.63	0.328	0.440
f7a9a9ac6	13.11	0.247	0.529	13.14	0.253	0.473	13.76	0.260	0.530	16.34	0.388	0.416
fb2c0499c2	14.93	0.442	0.469	15.61	0.481	0.375	16.38	0.530	0.381	19.14	0.608	0.284
fb3b73f1d3	11.78	0.132	0.622	11.72	0.125	0.610	12.80	0.180	0.630	13.41	0.189	0.588
ff59239865	12.35	0.432	0.533	12.81	0.420	0.481	14.28	0.455	0.493	17.72	0.516	0.395
average	14.12	0.405	0.509	14.14	0.419	0.455	14.56	0.453	0.486	16.72	0.520	0.399

Table 7: Per-scene 3DGS artifact restoration quantitative comparison on DL3DV-Res (Part 2).

	Difix3D+			GenFusion			GSFixer (Ours)		
	PSNR \uparrow	SSIM \uparrow	LPIPS \downarrow	PSNR \uparrow	SSIM \uparrow	LPIPS \downarrow	PSNR \uparrow	SSIM \uparrow	LPIPS \downarrow
0bfd020cf	15.96	0.498	0.494	15.16	0.511	0.510	17.04	0.526	0.476
2beaca3189	14.33	0.401	0.423	13.31	0.380	0.546	14.78	0.457	0.526
5a69d1027b	14.70	0.359	0.452	15.49	0.407	0.514	16.56	0.435	0.465
9c8c0e0fad	11.50	0.260	0.605	12.10	0.306	0.648	13.77	0.343	0.623
032dee9fb0	15.66	0.528	0.509	12.74	0.506	0.489	16.57	0.565	0.455
85cd0e9211	17.78	0.550	0.383	16.96	0.580	0.437	18.03	0.578	0.441
91afb9910b	14.09	0.508	0.518	15.14	0.576	0.481	16.20	0.589	0.485
165f5af8bf	16.49	0.476	0.395	15.63	0.496	0.458	16.85	0.516	0.439
374ffd0c5f	18.62	0.639	0.418	18.72	0.669	0.404	20.03	0.692	0.393
457e9a1ae7	16.28	0.583	0.458	17.13	0.640	0.417	18.33	0.660	0.416
669c36225b	12.01	0.449	0.576	11.78	0.496	0.539	13.28	0.503	0.527
9641a1ed79	15.37	0.610	0.621	15.19	0.615	0.517	16.46	0.612	0.495
56452d9cd9	13.76	0.400	0.549	13.74	0.418	0.526	14.93	0.420	0.513
493816813d	14.91	0.358	0.404	14.91	0.414	0.485	16.49	0.612	0.496
0853979305	18.31	0.630	0.368	17.21	0.653	0.417	18.62	0.671	0.394
adb95f29c1	14.07	0.427	0.538	13.09	0.452	0.565	15.24	0.485	0.550
b3bf9079b4	15.43	0.555	0.374	15.07	0.583	0.394	16.79	0.590	0.396
ba55c875d2	17.18	0.613	0.386	16.02	0.600	0.421	18.10	0.635	0.397
d1b3a0b37a	13.90	0.443	0.527	13.39	0.456	0.523	14.78	0.486	0.520
d904ae2998	12.94	0.439	0.647	10.92	0.344	0.593	13.06	0.416	0.568
dac9796dd6	13.90	0.561	0.518	14.29	0.559	0.453	15.79	0.610	0.443
dafa9c7cbd	11.68	0.169	0.497	11.81	0.224	0.643	12.64	0.250	0.624
df29c22586	19.31	0.538	0.238	19.84	0.585	0.370	21.13	0.633	0.318
e9360e7a89	14.50	0.463	0.490	13.52	0.446	0.508	14.82	0.492	0.526
ec305787b7	14.23	0.587	0.515	13.37	0.511	0.435	15.44	0.640	0.413
ed16328235	14.83	0.281	0.485	13.58	0.306	0.606	15.83	0.355	0.573
f004c810d9	17.53	0.729	0.314	17.76	0.757	0.321	18.85	0.763	0.325
ff59239865	12.56	0.416	0.547	12.09	0.443	0.583	13.51	0.467	0.574
average	15.07	0.4816	0.473	14.64	0.498	0.493	16.21	0.536	0.478

Table 8: Comparison of per-scene 3D reconstruction results of DL3DV with 3 input views.

	Difix3D+			GenFusion			GSFixer (Ours)		
	PSNR \uparrow	SSIM \uparrow	LPIPS \downarrow	PSNR \uparrow	SSIM \uparrow	LPIPS \downarrow	PSNR \uparrow	SSIM \uparrow	LPIPS \downarrow
0bfd020cf	17.54	0.547	0.394	17.39	0.584	0.405	18.21	0.582	0.399
2beaca3189	17.56	0.592	0.250	18.39	0.638	0.359	18.37	0.627	0.361
5a69d1027b	17.35	0.471	0.322	16.97	0.501	0.407	18.47	0.516	0.365
9c8c0e0fad	15.15	0.342	0.425	14.69	0.378	0.535	16.14	0.399	0.472
032dee9fb0	20.48	0.690	0.265	19.65	0.727	0.293	21.13	0.722	0.285
85cd0e9211	20.60	0.673	0.258	20.14	0.692	0.337	22.32	0.754	0.266
91afb9910b	17.56	0.622	0.346	18.53	0.673	0.366	18.64	0.672	0.365
165f5af8bf	18.06	0.551	0.302	17.76	0.570	0.374	18.71	0.576	0.349
374ffd0c5f	23.98	0.807	0.195	24.29	0.827	0.224	24.50	0.819	0.227
457e9a1ae7	19.48	0.694	0.347	20.48	0.752	0.322	20.93	0.735	0.343
669c36225b	15.42	0.566	0.400	16.24	0.300	0.396	16.64	0.612	0.412
9641a1ed79	18.05	0.658	0.470	18.17	0.668	0.418	18.47	0.651	0.419
56452d9cd9	16.35	0.422	0.409	17.70	0.511	0.420	18.84	0.562	0.373
493816813d	16.89	0.482	0.326	16.93	0.515	0.406	17.54	0.522	0.401
0853979305	22.35	0.771	0.212	22.39	0.807	0.245	22.71	0.789	0.260
adb95f29c1	16.78	0.516	0.435	15.73	0.526	0.482	18.87	0.583	0.383
b3bf9079b4	18.84	0.662	0.253	18.29	0.696	0.296	18.56	0.676	0.301
ba55c875d2	20.78	0.742	0.227	20.18	0.764	0.273	21.37	0.751	0.265
d1b3a0b37a	16.22	0.516	0.435	16.82	0.566	0.426	16.66	0.538	0.450
d904ae2998	14.36	0.480	0.541	13.10	0.446	0.533	13.97	0.480	0.526
dac9796dd6	19.83	0.735	0.285	20.63	0.767	0.278	20.87	0.768	0.279
dafa9c7cbd	13.32	0.226	0.418	13.29	0.270	0.573	14.21	0.279	0.541
df29c22586	24.24	0.713	0.150	24.64	0.737	0.256	24.57	0.724	0.216
e9360e7a89	15.80	0.540	0.372	15.63	0.559	0.426	16.09	0.569	0.430
ec305787b7	18.53	0.701	0.310	19.27	0.733	0.299	19.01	0.723	0.309
ed16328235	16.18	0.358	0.382	16.29	0.398	0.504	16.50	0.400	0.502
f004c810d9	22.77	0.859	0.157	22.94	0.872	0.202	23.62	0.874	0.194
ff59239865	16.89	0.549	0.339	17.59	0.611	0.403	19.05	0.600	0.378
average	18.26	0.5895	0.329	18.36	0.610	0.374	19.11	0.625	0.360

Table 9: Comparison of per-scene 3D reconstruction results of DL3DV with 6 input views.

	Difix3D+			GenFusion			GSFixer (Ours)		
	PSNR \uparrow	SSIM \uparrow	LPIPS \downarrow	PSNR \uparrow	SSIM \uparrow	LPIPS \downarrow	PSNR \uparrow	SSIM \uparrow	LPIPS \downarrow
0bfd020cf	19.15	0.582	0.320	19.70	0.635	0.366	20.03	0.605	0.352
2beaca3189	19.79	0.694	0.185	20.52	0.725	0.284	20.20	0.706	0.286
5a69d1027b	18.69	0.542	0.270	18.80	0.578	0.356	19.83	0.581	0.316
9c8c0e0fad	16.76	0.411	0.380	16.67	0.442	0.482	17.35	0.442	0.436
032dee9fb0	22.93	0.787	0.169	22.73	0.829	0.211	22.89	0.801	0.209
85cd0e9211	22.88	0.762	0.174	22.60	0.778	0.267	22.48	0.757	0.262
91afb9910b	20.45	0.715	0.248	20.28	0.737	0.301	20.51	0.733	0.295
165f5af8bf	19.41	0.597	0.255	19.12	0.617	0.330	19.67	0.611	0.316
374ffd0c5f	26.67	0.871	0.120	27.01	0.886	0.163	26.67	0.874	0.160
457e9a1ae7	21.66	0.761	0.262	22.05	0.800	0.281	22.21	0.777	0.299
669c36225b	17.03	0.636	0.324	17.91	0.690	0.336	17.60	0.656	0.362
9641a1ed79	18.85	0.675	0.419	19.30	0.702	0.389	19.32	0.676	0.389
56452d9cd9	17.32	0.473	0.393	19.01	0.594	0.370	19.29	0.561	0.372
493816813d	18.35	0.563	0.249	18.11	0.581	0.338	18.88	0.596	0.324
0853979305	24.54	0.835	0.152	24.66	0.856	0.192	24.86	0.841	0.199
adb95f29c1	18.29	0.557	0.343	18.17	0.598	0.399	18.88	0.584	0.383
b3bf9079b4	19.37	0.717	0.212	19.76	0.762	0.247	19.87	0.737	0.254
ba55c875d2	22.98	0.808	0.170	22.79	0.825	0.207	23.79	0.818	0.200
d1b3a0b37a	18.41	0.607	0.315	18.97	0.660	0.332	19.06	0.623	0.355
d904ae2998	16.80	0.548	0.408	16.03	0.548	0.443	16.71	0.553	0.430
dac9796dd6	22.06	0.807	0.207	22.00	0.815	0.232	22.42	0.812	0.231
dafa9c7cbd	14.33	0.276	0.385	13.92	0.297	0.533	14.80	0.309	0.512
df29c22586	25.66	0.759	0.115	26.14	0.782	0.228	26.01	0.774	0.172
e9360e7a89	17.95	0.626	0.289	18.66	0.668	0.339	18.15	0.643	0.352
ec305787b7	21.07	0.776	0.203	21.65	0.806	0.220	21.54	0.790	0.224
ed16328235	18.44	0.460	0.295	17.98	0.477	0.417	18.18	0.467	0.414
f004c810d9	25.11	0.899	0.126	25.50	0.911	0.157	25.40	0.906	0.157
ff59239865	18.37	0.613	0.272	18.88	0.658	0.369	20.13	0.654	0.333
average	20.12	0.656	0.259	20.32	0.688	0.314	20.60	0.675	0.307

Table 10: Comparison of per-scene 3D reconstruction results of DL3DV with 9 input views.

	Difix3D+			GenFusion			GSFixer (Ours)		
	PSNR \uparrow	SSIM \uparrow	LPIPS \downarrow	PSNR \uparrow	SSIM \uparrow	LPIPS \downarrow	PSNR \uparrow	SSIM \uparrow	LPIPS \downarrow
3 Views									
bicycle	13.02	0.177	0.632	14.75	0.247	0.632	15.80	0.284	0.613
bonsai	13.86	0.397	0.549	13.87	0.408	0.549	13.42	0.434	0.554
counter	13.96	0.394	0.519	15.20	0.470	0.519	15.25	0.472	0.505
flowers	11.81	0.154	0.693	12.86	0.202	0.693	13.80	0.288	0.654
garden	14.34	0.258	0.573	16.13	0.289	0.573	17.42	0.326	0.537
kitchen	15.56	0.371	0.537	16.14	0.419	0.537	16.61	0.424	0.503
room	14.15	0.465	0.427	16.23	0.568	0.427	15.54	0.540	0.441
stump	15.35	0.215	0.620	16.51	0.296	0.620	17.62	0.320	0.603
treehill	13.19	0.253	0.649	13.57	0.311	0.649	15.03	0.319	0.619
average	13.92	0.298	0.578	15.03	0.357	0.578	15.61	0.370	0.559
6 Views									
bicycle	15.58	0.253	0.594	16.16	0.292	0.570	17.32	0.302	0.549
bonsai	16.30	0.525	0.427	17.08	0.545	0.426	17.29	0.556	0.440
counter	16.09	0.490	0.413	17.06	0.545	0.426	17.12	0.530	0.425
flowers	12.66	0.178	0.572	13.69	0.224	0.632	14.10	0.216	0.594
garden	17.58	0.360	0.363	18.62	0.396	0.452	18.98	0.400	0.429
kitchen	17.95	0.534	0.310	18.62	0.556	0.388	18.78	0.555	0.371
room	15.07	0.525	0.460	17.73	0.628	0.387	16.76	0.606	0.403
stump	17.51	0.284	0.485	17.77	0.321	0.570	18.65	0.328	0.543
treehill	14.70	0.293	0.588	15.36	0.353	0.585	16.46	0.341	0.546
average	15.94	0.382	0.468	16.90	0.430	0.494	17.27	0.426	0.478
9 Views									
bicycle	16.99	0.288	0.498	16.89	0.313	0.541	17.89	0.322	0.511
bonsai	18.54	0.661	0.343	19.43	0.661	0.343	19.53	0.654	0.356
counter	17.42	0.552	0.352	18.18	0.607	0.368	18.82	0.600	0.362
flowers	13.97	0.218	0.499	14.50	0.253	0.593	14.98	0.244	0.534
garden	19.18	0.453	0.282	19.79	0.471	0.393	20.10	0.473	0.367
kitchen	20.08	0.610	0.243	20.56	0.635	0.316	20.58	0.623	0.314
room	17.96	0.626	0.343	19.72	0.700	0.317	18.96	0.666	0.333
stump	18.50	0.340	0.425	19.09	0.376	0.522	19.59	0.378	0.496
treehill	15.25	0.322	0.537	16.42	0.387	0.566	17.24	0.366	0.507
average	17.54	0.452	0.391	18.29	0.489	0.507	18.63	0.481	0.420

Table 11: Per-scene 3D sparse view reconstruction quantitative comparison on Mip-NeRF 360.